CELL OF ORIGIN IN PANCREATIC DUCTAL ADENOCARCINOMA

by

ALEX Y.L. LEE

B.Sc., The University of British Columbia, 2014

A THESIS SUBMTITED IN PARTIAL FULFILLMENT OF THE REQUIREMENTS FOR THE DEGREE OF

MASTER OF SCIENCE

in

THE FACULTY OF GRADUATE AND POSTDOCTORAL STUDIES

(Cell and Developmental Biology)

THE UNIVERSITY OF BRITISH COLUMBIA

(Vancouver)

April 2017

Abstract

Pancreatic ductal adenocarcinoma (PDAC) is a deadly disease with a ductal morphology. Prior research has identified both pancreatic acinar and ductal cells as possible cells of origin for histologically similar PDAC. However, because different mutations were induced in acinar and ductal cells, apt comparisons could not be made to address whether the tumor cell of origin influences PDAC initiation, development, and other tumor differences. To address this open question, I induced oncogenic Ras expression ($Kras^{G12D}$) with concomitant homozgyous *Trp53* deletion at 4 weeks of age in a ductal cell specific (*Sox9CreER*; $Kras^{LSL\text{-}G12D}$; $Trp53^{flox/flox}$ ("$Duct{:}KP^{cKO}$")) and an acinar cell specific ($Ptf1a^{CreER}$; $Kras^{LSL\text{-}G12D}$; $Trp53^{flox/flox}$ ("$Acinar{:}KP^{cKO}$")) mouse model. I found that $Duct{:}KP^{cKO}$ mice met their humane endpoints earlier (82 days post injection, p.i.) than the $Acinar{:}KP^{cKO}$ mice (128 days p.i.), for reasons associated with differences in the timing of PDAC onset. While tumors from both cells of origin were similarly proliferative and shared many physical characteristics, $Duct{:}KP^{cKO}$ mice developed tumors much earlier than $Acinar{:}KP^{cKO}$ mice and this was further associated with a difference in precursor lesion initiation. Specifically, ductal cells only formed high-grade lesions while acinar cells formed precursor lesions of all grades. These findings suggest that cell type intrinsic differences may allow ductal cells to rapidly form PDAC under genetically favorable conditions. In comparison, acinar cells likely require additional steps to alter cell identity and become duct-like – thus delaying PDAC initiation and extending survival. Taken together, I have demonstrated, by using cell type specific mouse models, that cell of origin can alter disease initiation, progression and impact PDAC phenotype.

Preface

The overall research objectives described in this thesis were developed in collaboration with Dr. Janel Kopp, Dr. Calvin Roskelley, Dr. Cathy van Raamsdonk and the author, Alex Lee. Experiments were designed and executed by Alex Lee in consultation with Dr. Janel Kopp. Husbandry for fourteen mice in this study from the survival and timepoint analysis, described in chapters 3.1, 3.4 and 3.5, were conducted at the University of California, San Diego (UCSD), by Dr. Janel Kopp. Images and data for the recombination specificity analysis were conducted by Claire Dubois also at the University of California, San Diego. These experiments were in full compliance of all protocols as approved by the San Diego Animal Care and Use Committees. All other mice described in this study were bred and handled by Alex Lee with technical support from our laboratory technician, Yu Cao, as well as the staff of the Modified Barrier Facility (MBF). These latter animal experiments were approved by the University of British Columbia Animal Care and Use Committees. Analysis of all data was done by Alex Lee in consultation with Dr. Janel Kopp and Dr. David Schaeffer (trained pathologist).

CCAC experimental animal user program certificate #: 6917-14

Biology and Husbandry of the Laboratory Rodent certificate #: RBH-164-14

Anesthesia of the laboratory rodent certificate #: RA-82-14

Table of Contents

List of Tables

List of Figures

List of Abbreviations

AC – acinar cell

Acinar:KP^{cKO} – Ptf1a^{CreER}; Kras$^{LSL\text{-}G12D/+}$; Trp53$^{flox/flox}$ acinar cell specific conditional knockout mouse model

ADM – acinar-to-ductal metaplasia

BSA – bovine serum albumin

CAC – centroacinar cell

CAII – carbonic anhydrase ii

CC3 – cleaved caspase 3

CDKN2A – cyclin dependent kinase inhibitor 2A

CK19 – cytokeratin 19

CreER (CreERT) – cre recombinase, estrogen receptor conjugated

DAB – 3,3'-diaminobenzidine tetrahydrochloride

Dox – doxycycline

Duct:KP^{cKO} – Sox9CreER; Kras$^{LSL\text{-}G12D/+}$; Trp53$^{flox/flox}$ ductal cell specific conditional knockout mouse model

EDTA – ethylenediaminetetraacetic acid

EGF – epidermal growth factor

Elas-tTA – elastase driven tetracycline transactivator

FFPE – formalin fixed paraffin embedded

FGF – fibroblast growth factor

GFP – green fluorescence protein

GOF – gain of function

H&E – hematoxylin and eosin

IgG – immunoglobulin G

IHC – immunohistochemistry

Kras – Kirsten rat sarcoma viral oncogene homolog

LOF – loss of function

LSL – loxp-stop-loxp

MAPK – mitogen activated protein kinase

mPanIN – mouse pancreatic intraepithelial neoplasia or neoplasms

NDS – normal donkey serum

PanIN – pancreatic intraepithelial neoplasia or neoplasms (human)

PBS – phosphate buffered saline

PCR – polymerase chain reaction

PDAC – pancreatic ductal adenocarcinoma

PDX1 – pancreatic and duodenal homeobox 1

PTF1A – pancreas transcription factor 1 subunit alpha

SEM – standard error of the mean

SMAD4 – mothers against decapentaplegic homolog 4

TBS – tris buffered saline

tetO-Cre – tetracycline operator driven cre recombinase

TGF – transforming growth factor

TM – tamoxifen

TP53 (*Trp53*) – tumor protein p53

YFP – yellow fluorescence protein

Acknowledgements

The acknowledgements, a chapter in my thesis dedicated for thanks and to reflect on the relationships and conversations, the “non-cell autonomous signaling” within my lab and LSI microenvironment, so to speak, which have made this possible.

First and foremost, I would like to thank my supervisor and mentor, Dr. Janel Kopp, for offering me the opportunity to learn from her, for always being eager to teach, and for fostering a supportive, collaborative and caring laboratory working environment. I am forever grateful for the guidance and insight she has provided me, especially with experimental design, critical thinking and scientific communication – all skills that will surely play an important role in my future endeavors. Her dedication and expertise with this craft never ceases to amaze. Second, I would like to thank my supervisory committee, Dr. Calvin Roskelley and Dr. Cathy van Raamsdonk for their helpful and invaluable advice navigating through the successes and difficulties in my graduate student life. In addition, I would like to thank Dr. David Schaeffer for his assistance with all matters pathology and Dr. Maike Sander (Sander Lab, UCSD) for her early support with this research. Finally, I would like to thank all past (The Penultimate Chancellor “Yu” (Jason) Cao, Karnjit) and current (Andy, Atefeh, Soheila) lab members for their company, conversations and insightful advice in all matters of life and lab.

Outside of the lab, I would also like to thank the friends that I have made as well as my family for their unconditional support of me and my studies.

Chapter 1. Introduction

1.1 Overview

Cancers with a common histology can sometimes come from different cells of origin, which can lead to cancer heterogeneity, phenotype and development differences (Blanpain, 2013; Visvader, 2011). Despite the histological similarity, the cell of origin can influence cancer subtype, signaling, progression, and phenotype of cancers that emerge (Blanpain, 2013; Visvader, 2011). This leads to the tantalizing possibility that by elucidating the cell of origin specific effects on cancer, we may eventually allow for personalized treatments that could improve patient survival. This is of particular importance for deadly cancers such as pancreatic ductal adenocarcinoma (PDAC), on which this thesis is focused. However, before these ambitions can come to fruition, a basic understanding of how different cell types contribute to PDAC must be attained. Therefore, I sought to first determine the effect of simultaneous $Kras^{G12D}$ expression and *Trp53* deletion on both ductal and acinar cells of the pancreas, and second, to determine how these distinct cells of origin may impact tumor initiation, development and other tumor characteristics. This thesis describes experiments that provide one of the first descriptions of how cell of origin affects PDAC development when identical genetic initiating events are present, and lay the foundation for understanding how cell of origin can impact PDAC. Ultimately, continued research may elucidate specific cell of origin derived transcriptome profiles that could inform PDAC cell of origin in patients and potentially lead to improvements in precision medicine for this deadly disease.

1.2 Pancreatic ductal adenocarcinoma (PDAC)

Cancer is a leading cause of death worldwide, and pancreatic cancer is projected to be the deadliest cancer by 2030, if early diagnosis or therapeutic efficacy does not dramatically improve (Rahib et al., 2014). Currently, the 5-year relative survival rate for a PDAC patient is approximately 9% in the United States of America (Howlader et al., 2016). This poor outcome reflects the difficulty of diagnosing and treating PDAC. For instance, over 50% of patients have metastatic PDAC at diagnosis, and even those fortunate enough to be diagnosed early with localized PDAC still only have a 30% relative 5-year survival rate (Howlader et al., 2016). Therefore, finding ways to detect PDAC early and enhance treatment response are two essential strategies needed to improve patient survival.

The most commonly accepted model of PDAC development proposes that cancer arises primarily from undetectable microscopic lesions known as pancreatic intraepithelial neoplasms (PanINs) (Andea et al., 2003). One model for PanIN development posits that low-grade precursor lesions, known as PanIN1s, are initiated by acquiring oncogenic driver mutations, such as those in *Kras*, a GTPase protein in the MAP kinase signaling pathway. These lesions then accumulate additional mutations, leading to increasing cellular atypia through stages PanIN2 and PanIN3 before becoming invasive PDAC (Figure 1.1). The basis of this model of PanIN development largely stems from the following key observations: 1) that PanIN1 lesions are increasingly observed with age (Schwartz and Henson, 2007), 2) that PanIN lesions, like PDAC, show similar enrichment patterns in the pancreatic head, the area adjacent to the duodenum (Andea et al., 2003; Cubilla and Fitzgerald, 1976; Kozuka et al., 1979), 3) that high-grade lesions are found more frequently in patients with PDAC than without (Andea et al., 2003), and finally, 4) that PanIN lesions show a progressive

accumulation of mutations in genes commonly mutated in PDAC, such as *KRAS*, *CDKN2A*, *TP53*, and *SMAD4*, concordant with increases in histological grade (Hruban et al., 2000, 2008) (Figure 1.1). Despite these findings, no studies have comparatively addressed whether and how PDAC development from different pancreatic cells of origin may impact PanIN initiation and progression.

Improvements in treatment responses in PDAC over the past decades have been scarce, with only meager gains in survival with the advent of each new chemotherapeutic regimen (Teague et al., 2015). Considering this, researchers are looking for alternatives to broad-spectrum anti-cancer agents and are trying to develop personalized molecular medicine approaches that would target specific cancer subtypes. This is of particular interest due to demonstrations in breast cancer that proper molecular subtyping has allowed rapid improvements in survival, simply by tailoring treatments to specific subtypes (Schnitt, 2010; Yersal and Barutca, 2014). Such improvements require fundamental research to identify major subtypes that are clinically relevant and actionable for each disease.

1.3 Heterogeneity in PDAC

To mirror successes seen in the molecular subtyping of breast cancer, PDAC needs to be classified into clinically relevant subtypes. To this end, numerous groups have published expression profile studies of PDAC that suggest the existence of subtypes, however, the characteristics and clinical relevance of each are still debated (Bailey et al., 2016b; Collisson et al., 2011; Moffitt et al., 2015; Noll et al., 2016). The first study to attempt characterization of PDAC heterogeneity identified 3 main subtypes: classical, exocrine-like and quasi-mesenchymal. The first two subtypes exhibited enriched expression of epithelial/cell-cell adhesion genes, and genes associated with exocrine function, respectively. The latter subtype

showed increased expression of mesenchymal genes. Importantly, classical and exocrine-like subtypes were differentially sensitive to various chemotherapeutic agents (Collisson et al., 2011; Noll et al., 2016) and thus could be clinically relevant. Follow-up studies, which employed alternate experimental methods, continued to refine and incorporate new subtypes (Bailey et al., 2016b; Collisson et al., 2011; Moffitt et al., 2015). Although these studies have so far failed to reach a consensus regarding the defining characteristics of a given subtype, these reports collectively suggested the existence of at least 2 tumor epithelial cell subtypes – but the mechanism underlying the development of these distinct subtypes is unknown.

1.4 Cell of origin derived effects on cancer

Cancers are frequently heterogeneous within a population, presenting with different phenotypes or genotypes between patients. These differences are hypothesized to emerge through various possible mechanisms. For instance, heterogeneity may emerge stochastically, from differences in selective pressure (eg. from the peritumoral microenvironment or from specific molecular alterations acquired by the tumor cells) or from differences in cellular origin (ie. the first cell to acquire the cancer initiating mutation). While all of these processes are likely sources of interpatient tumor heterogeneity, one possibility stands out for pancreatic cancer – cell of origin derived heterogeneity. The expression profile study published by Collisson et. al. (2011) showed a potential role for cell of origin in PDAC heterogeneity by identifying PDAC subtypes that expressed genes highly enriched in normal ductal (ie. the classical subtype) or acinar cells (ie. the exocrine-like subtype). It is possible that these differences are caused by remnants from the transcriptional programming of the cell of origin (Collisson et al., 2011). Although it is seemingly counter-intuitive that acinar cells may initiate ductal adenocarcinomas, studies from as early as two decades ago have

demonstrated that acinar cells can change their differentiation status under certain conditions (Wagner et al., 1998). To address the possibility that PDAC can emerge from different cells of origin, proper animal models are needed to generate tumors derived from different cells of origin. Cell type specific animal models have been a powerful research tool in other cancers, one of them being prostate cancer.

Like the pancreas, the prostate has two different epithelial cell types that may give rise to adenocarcinomas. Thus, researchers sought to examine: 1) whether luminal and basal cells both contribute to prostate cancer under disease relevant *in vivo* conditions, and 2) whether and how cell of origin impacts tumor development, phenotype and survival. To address these questions, researchers developed cell-type specific mouse models that enabled finer spatial targeting of pro-tumorigenic mutations to either basal or luminal cells of the prostate. Specifically, these studies applied identical disease relevant mutations (homozygous *Pten* deletion) to observe for cell of origin derived effects in prostate cancer. Their findings showed conclusively that both luminal and basal cells can give rise to prostate cancer of similar luminal histology. Therefore, due to cellular plasticity, tumor histology should not be used as an indicator of cancer cell of origin (Choi et al., 2012; Lu et al., 2013; Park et al., 2016; Wang et al., 2013). Further analysis revealed subtle differences in the timing of tumor development from luminal and basal cells. Specifically, these studies found that luminal cells initiated and developed into prostate cancer much more quickly when compared to basal cells carrying the same $Pten^{flox/flox}$ mutations (Choi et al., 2012; Wang et al., 2013). This difference was attributed to basal cells requiring a transition into a luminal-like cell prior to initiating prostate cancer (Choi et al., 2012). Moreover, molecular analyses revealed that although tumors arising from both cells of origin were overall similar, subtype specific

signatures could nevertheless be generated and applied to human transcriptome data (Wang et al., 2013). By comparing tumors with different cell type specific signatures in patients, the authors found that tumors associated with a luminal cell of origin signature were associated with more aggressive prostate cancers with reduced patient survival times (Wang et al., 2013), suggesting that 1) cell of origin differences may persist after tumor initiation, and that, 2) cell of origin studies may identify specific tumor signatures that have not been found through traditional human tumor analyses alone, providing an additional avenue with which to examine potential sources of tumor heterogeneity.

In addition to the prostate, cell of origin has also been shown to play a role in cancers from numerous other organs, such as in the brain, breast, and lung (Blanpain, 2013). Briefly, by only changing the cell of origin while inducing identical mutations, cell of origin has been found to affect signaling pathway activation (brain cancer), histological subtypes (lung cancer), molecular subtypes (breast cancer) and disease prognosis (prostate, breast, and brain cancer). Thus, the importance of studying cell of origin should not be understated, and has been demonstrated in many cancers. However, the effect and relevance of cell of origin in pancreatic cancer remain largely unknown and understudied.

1.5 Cell of origin of PDAC

The pancreas has two major types of cells: exocrine and endocrine islet cells. The former includes ductal and acinar cells, while the latter is composed of a variety of hormone secreting cells. Despite the variety of distinct cell types, the majority of pancreatic cancers are ductal adenocarcinomas. One reason for this may be that pancreatic ductal cells are the most susceptible to oncogenic transformation. However, clinical evidence supporting this notion is limited and largely correlative. For instance, ductal abnormalities (eg. hyperplasia

and metaplasia) are frequently associated with PDAC, but rarely detected prior to PDAC initiation because of their microscopic size (Brat et al., 1998; Brockie et al., 1998; Cubilla and Fitzgerald, 1976; Furukawa et al., 1994, 1994, Kozuka et al., 1979, 1979). Due to technical challenges involved in following PDAC tumor initiation and development in humans, mouse models are needed to study these events. The majority of early inducible PDAC models were pan-pancreatic (that is, they involved all cells of the pancreas) because they were dependent on embryonic induction of constitutive Cre recombinase alleles driven by the *Pdx1* or *Ptf1a* promoters, and thus offered no pancreatic cell type specificity (Hingorani et al., 2003). However, in one of the earliest studies employing cell type specific modeling of PDAC, Wagner et al. (1998) found that *Elastase* promoter driven TGFα expression (resulting in overactivation of the Kras kinase cascade) induced acinar cells to become more like ductal cells, and PDAC development after a considerable latency (Wagner et al., 1998). A follow up study deleting *Trp53* in conjunction with TGFα overexpression in acinar cells found that survival was significantly shortened due to the rapid onset of PDAC (Wagner et al., 2001). In contrast, oncogenic $Kras^{G12V}$ expression, specifically in ductal cells, induced only mild phenotypic changes after 6 months (Brembeck et al., 2003). Therefore, these studies made a case for an acinar cell of origin of PDAC by suggesting that 1) acinar cells can give rise to PDAC in mice, and that 2) the hyperplastic and metaplastic ductal lesions previously thought to derive from ductal cells and associated with PDAC, could actually be derived from acinar cells instead (Hruban et al., 2000).

Subsequently, the role of acinar cells in PDAC initiation and progression continued to be refined. Tamoxifen-inducible mouse models were developed to drive acinar cell specific expression of oncogenic Kras using different promoters such as: *Ptf1a*, *Mist1* and *Cela*

(elastase) (De La O et al., 2008; Guerra et al., 2007; Habbe et al., 2008, 2008; Ji et al., 2009; Kopinke et al., 2012; Kopp et al., 2012). These models showed that mPanIN lesions readily arose from acinar cells, through a process that could be hastened by the application of pancreatitis (Guerra et al., 2007; Kopp et al., 2012). Acinar cell transdifferentiation to a duct-like cellular identity coincided with concomitant down regulation of acinar cell specifying factors and reactivation of a progenitor/ductal cell-like transcription program (De La O et al., 2008; Kopp et al., 2012; Krah et al., 2015; Morris et al., 2010; Pinho et al., 2011a, 2011b; Roy et al., 2016; Shi et al., 2009). Cumulatively, these reports provided insight into the early stages of acinar cell transdifferentiation, but few reports extended these observations to the role of acinar cells in PDAC induction (Bailey et al., 2016a; Daniluk et al., 2012; Guerra et al., 2007, 2011; Swidnicka-Siergiejko et al., 2016).

Ductal cells have received far less attention than acinar cells due to the technical challenges of specifically targeting this cell population, as well as the initial observation that this cell type appeared to be refractory to the effects of oncogenic Kras (Brembeck et al., 2003). Since the earliest *CK19-Kras*^{G12V} report by Brembeck et al. (2003), other ductal cell specific models have emerged, utilizing various ductal cell specific promoters: *Ck19*^{CreER}, *Hnf1bCreER*, *CAIICreER* and *Sox9CreER* (Inada et al., 2008; Kopp et al., 2011; Means et al., 2008; Solar et al., 2009). Experiments combining the transgenic *Sox9CreER* or knock-in *CK19*^{CreER} models with a Cre-inducible oncogenic Kras allele have shown that ductal cells can give rise to rare mPanIN lesions (Kopp et al., 2012; Ray et al., 2011), but to a much lesser degree than acinar cells – an 112 fold difference according to Kopp et al. (2012). Despite the progress made to show that ductal cells can give rise to lesions resembling

mPanIN1, the tumorigenic potential and similarities of these ductal cell-derived lesions compared to acinar cell derived mPanIN or even human PanINs remain unknown.

Direct comparisons between acinar and ductal cells as potential PDAC cells of origin have only begun to be addressed (Figura et al., 2014a; Kopp et al., 2012). Although ductal cells have been shown to give rise to mPanINs (Kopp et al., 2012; Ray et al., 2011), it hasn't been demonstrated whether these ductal cell derived lesions progress in the same manner as acinar cell derived mPanIN, or whether they are viable as a cell of origin for PDAC. A study by Bailey et al. (2016a) found that tumor development from $Kras^{G12D}$-expressing ductal and acinar cells required differing doses of gain-of-function $Trp53^{R172H}$ when expressed with oncogenic Kras. Furthermore, they reported a complete absence of mPanIN lesions from the ductal cell specific mouse line, but numerous mPanINs from the acinar cell specific mouse line. This suggested a potential difference in PDAC development from ductal cells and acinar cells, but due to differences in genetics, cell of origin effects alone could not be confidently attributed to this difference in tumor development. In addition, alcian blue, a mucin stain, was used to identify mPanIN lesions even though precursor lesions do not have to be mucinous, especially at higher mPanIN grades. Instead, PanIN/mPanIN lesions are defined morphologically by specific cytological features and not solely by alcian blue staining (Figure 1.1). Therefore, a histologically guided study using genetically comparable models that initiate PDAC from distinct cell of origins is needed, to directly address the effects of cell of origin on PDAC initiation, development and phenotype.

1.6 Hypothesis

I hypothesize that concomitant $Kras^{G12D}$ expression and homozygous *Trp53* loss in either acinar or ductal cells will induce pancreatic ductal adenocarcinoma in mice. However,

because acinar cells need to acquire a ductal-cell-like fate before contributing to PDAC, tumor development will be delayed from acinar compared to ductal cells.

1.7 Objectives

To directly address the impact of cell of origin on PDAC and its implication for survival, tumor initiation and development, I generated cell type specific Cre-recombinase, tamoxifen inducible mouse models where identical genetic mutations were induced in ductal or acinar cells (*Sox9CreER*; *Kras*$^{LSL\text{-}G12D}$; *Trp53*$^{flox/flox}$ ("*Duct:KP*^{cKO}") or *Ptf1a*^{CreER}; *Kras*$^{LSL\text{-}G12D}$; *Trp53*$^{flox/flox}$ ("*Acinar:KP*^{cKO}")) mice, respectively). I specifically looked for differences in survival between cell type specific mouse lines and then examined whether cell of origin impacted tumor physical characteristics (number, size, and subsite localization), timing of tumor initiation/tumor growth, as well as the timing of precursor lesion initiation and accumulation. To study these aspects of tumorigenesis, I quantitatively analyzed H&E and immunohistochemically stained tissue from mice at humane endpoint or from early timepoints.

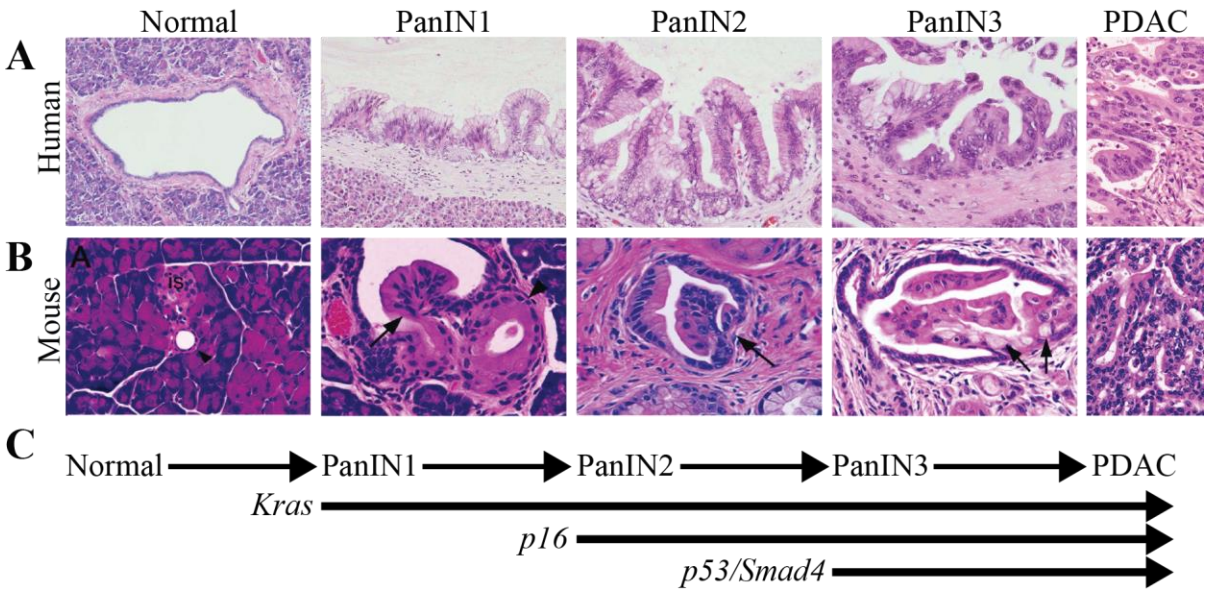

Figure 1.1 Comparison of human PanIN versus those from genetically engineered mouse models ("mPanIN").

Figure 1.1 Normal epithelium is characterized by lack of atypia, crowding, or cribiforming with a regular cellular arrangement. PanIN1/mPanIN1 display regular, basally located nuclei with tall columnar hypermucinous cells which may be papillary. PanIN2/mPanIN2 can be flat or papillary, but have additional nuclear abnormalities and rare mitoses can be seen. PanIN3/mPanIN3, or carcinoma-in-situ, display abundant nuclear atypia (enlargement, pleomorphism, hyperchromasia) and cribiforming, but are still bound by a basement membrane. PDAC is no longer bound in place by the basement membrane and has invaded beyond it. **A**) Representative figures of human PanINs, showing progression from normal epithelium to invasive PDAC. **B**) Mouse PanIN ("mPanIN") and PDAC observed in the *Pdx1-Cre*; *Kras*$^{LSL\text{-}G12D}$ mouse model (Hingorani et al., 2003). Black arrows specifically highlight the precursor lesions being referenced. **C**) The PanIN model of PDAC development proposes that mutations arise sequentially – with *KRAS* mutations being the earliest (PanIN1), *CDKN2A* (p16) intermediate (PanIN2) and *SMAD4* or *Trp53* being the latest (PanIN3 and PDAC) mutations observed. Figure 1.1A and 1.1B adapted from Hruban et al. (2001) and Hingorani et al. (2003) with permission.

Chapter 2. Materials and Methods

2.1 Mice

All described animal experiments were approved by the University of British Columbia and University of California, San Diego Animal Care and Use Committees. *Sox9CreER* (Font-Burgada et al., 2015; Kopp et al., 2011), *Kras*$^{LSL\text{-}G12D}$ (Tuveson et al., 2004), *Trp53*^{flox} (Marino et al., 2000), *R26R*$^{LSL\text{-}YFP}$ (Srinivas et al., 2001) and *Ptf1a*^{CreER} (Pan et al., 2013) mice have previously been described. Mice were maintained on a mixed C57BL6/CD1 background. Polymerase chain reaction (PCR) primers used to genotype animals, or confirm recombination are described in Table 2.1. CreER-mediated chromosomal recombination was achieved through administration of tamoxifen in corn oil (20mg/ml), delivered subcutaneously, every other day over 5 days at 0.125g tamoxifen/g body mass. Humane endpoint for survival analysis was defined by one of the following: presence of jaundice, body weight loss of ≥20% of the maximum weight obtained by the animal, severely altered activity levels, and/or impaired feeding/drinking. Eye irritation or enlarged lungs in *Sox9CreER; Kras*$^{LSL\text{-}G12D}$*; Trp53*$^{flox/flox}$*; R26R*$^{LSL\text{-}YFP}$ animals occasionally resulted in animals meeting humane endpoint; these animals were censored from the survival study (Figure 1C).

2.2 Histology and Morphometric Analysis

Pancreata were fixed overnight using Z-FIX (Anatech Ltd.) or 4% paraformaldehyde, then processed and embedded in paraffin. Paraffin-embedded tissues were sectioned into 5 or 7 μm-thick sections. Serial sections were collected until all lobes of the pancreas displayed maximal cross-sectional area (typically 420 μm in depth). From these serial sections, every 10th section was stained with hematoxylin and eosin (H&E) and examined microscopically.

For annotation of tumor number, size and location, one or more stained slides were selected as representative of the maximal pancreatic area and imaged with a 20x objective using an Aperio CS2 (Leica) or AxioScan (Zeiss) slide scanner. Whole slide images in figures were compiled by placing the image on a similarly colored background for presentation purposes and non-tissue artifacts were removed (eg. "+" symbols from charged slides).

Histological and morphometric analysis was conducted by Alex Lee (A.L.) and Dr. Janel L. Kopp (J.L.K.) independently and confirmed with Dr. David F. Schaeffer (D.F.S.) (trained pathologist). All data were plotted in Graphpad Prism unless otherwise specified. Physical characteristics of the pancreata/tumors were assessed in the following ways: 1) tumor size measurements were determined using the digital ruler tool in Aperio ImageScope. The cross-sectional diameter, in millimetres, of the tumors was measured between the two most distant edges of a neoplasm. To calculate mean tumor sizes for specific timepoints or at humane endpoint, average tumor sizes per mice were determined, then averaged across the experimental cohort/timepoint to arrive at a figure corresponding to the average tumor size. 2) Pancreata/tumor area measurements were determined by the selective masking of the tumor (tumor area) or all pancreatic tissue (total area) using Adobe Photoshop CC. The area of each was expressed as a pixel count and this was utilized to calculate the percentage area occupied by tumor per pancreas. 3) Tumor subsite analysis was accomplished by determining whether a tumor was qualitatively closer to the duodenum (head), pancreatic lymph nodes (body), or spleen (tail). If a sufficiently large tumor spanned two or more tumor sub-sites, the tumor was counted as being present in both sub-sites. This data was presented in a Radar diagram, which was plotted in Microsoft Excel as the percentage of tumors present in a subsite over the total tumor count from all subsites. 4) To analyze the type and number of precursor

lesions present in each mouse model, representative sections were selected from each animal and every gland with a lumen was categorized as one of the following: normal, acinar-to-ductal metaplasia (ADM), mPanIN1, mPanIN2, or mPanIN3. Glands representing more than one of these categories were scored according to their highest grade feature. Preneoplastic lesions directly adjacent to tumors or associated with visibly invasive cells were not included in this analysis. Invasive lesions were counted as small microtumors during the quantification of the tumor number.

2.3 Immunohistochemistry

Sections were deparaffinised with sequential xylene baths then rehydrated in ethanol-water solutions of gradually increasing water content. Antigens were unmasked using citrate buffer based (pH6.0) heat induced epitope retrieval. Peroxidase activity was quenched using 0.6% hydrogen peroxide in Tris buffered saline (TBS), pH7.6, at room temperature for 15 minutes, followed by a blocking and permeabilization step with 1% bovine serum albumin (BSA) and 10% normal donkey serum (NDS) in 0.025% triton-x100, TBS, pH7.6. Sections were incubated overnight at 4˚C with primary antibodies. Biotinylated secondary antibodies were incubated with the sections at room temperature for 1-2 hours before changing to VECTASTAIN Elite Avidin-biotin complex (ABC, Vector Labs) incubation at room temperature for 2-5 hours. 3-3'-diaminobenzidine tetrahydrochloride (DAB) was used as the chromogen. Slides were counter stained with Mayer's hematoxylin (Fisher) and mounted with Cytoseal (Fisher). Whole slide images of the staining were taken, as above, and analyzed using the annotation functions of the Aperio Imagescope software.

An alternate protocol was refined to immunohistochemically stain p53. Sections were deparaffinized and rehydrated, then subjected to extended heat induced epitope retrieval at

95˚C for 40 minutes in pH9, Tris-EDTA buffer (10mM Tris base, 1mM Ethylenediaminetetraacetic acid (EDTA) solution, 0.05% Tween 20). Peroxidase activity was quenched in 3% hydrogen peroxide in pH7.4 phosphate buffered saline (PBS). Mouse-on-mouse antibody block (Vector Labs) was applied (12µL/mL pH7.4, PBS buffer) for 1 hour at room temperature. Additional blocking (0.5% bovine serum albumin w/v, 5% NDS v/v, 0.3% Tween 20 v/v in pH7.4 PBS) at room temperature was carried out for 30 minutes before incubation with primary p53 antibody overnight, at 4˚C. The secondary antibody (Vector Labs IMMpress anti-mouse IgG diluted 1:1 in pH7.4, PBS) was incubated for 30 minutes at room temperature and stained, counterstained, and mounted as previously described.

2.4 Recombination specificity

Four weeks post tamoxifen injection, immunofluorescence analysis of recombination specificity was quantified in the acinar and ductal cell compartments, 4% paraformaldehyde fixed tissues were embedded in OCT (Tissue Tek) and cut into 10 µm sections. Tissues from *Sox9CreER; Trp53$^{flox/flox}$; R26R$^{LSL-YFP}$* and *Ptf1a^{CreER}; Trp53$^{flox/flox}$; R26R$^{LSL-YFP}$* mice (with and without the *Kras$^{LSL-G12D}$* allele) were stained with ductal and acinar cell specific markers (Sox9 and Cpa1, respectively), nuclear specific Hoechst dye and lineage reporter YFP and then quantified as previously described (Kopp et al., 2011, 2012).

2.5 Antibodies and reagents

The following primary antibodies were used to detect: CK19 (rabbit, Abcam Ab133492, 1:1000), GFP (rat, C. Kioussi, 1:1000 and goat, Abcam Ab6673, 1:200), Sox9 (rabbit, Chemicon,1:10,000 or guinea pig, Novo Nordisk, 1:1000), CPA1 (goat, R&D Systems, 1:1000), p53 (mouse, Cell Signaling Technologies 1C12, 1:500), Ki67 (rabbit, Thermo

Fisher SP6, 1:200), and cleaved caspase 3 (rabbit, Cell Signaling Technologies 5A1E, 1:1000). The secondary antibodies used include: biotin-conjugated horse anti-goat (Vector BA-9500, 1:500), biotin-conjugated donkey anti-rabbit (Jackson ImmunoResearch Laboratories 711-065-152, 1:500), Cy3-conjugated donkey anti-goat (Jackson ImmunoResearch Laboratories, 705-165-147, 1:500), Alexa488-conjugated donkey anti-goat (Jackson ImmunoResearch Laboratories, 705-545-003, 1:500) and donkey anti-mouse (Jackson ImmunoResearch Laboratories, 714-545-150, 1:500), and Cy5-conjugated donkey anti-guinea pig (Jackson ImmunoResearch Laboratories, 706-175-148, 1:500).

2.6 Statistical analysis

Significance and P-values were determined using two-tailed student's T-test in GraphPad Prism or Excel software. All data are presented as mean ± standard error of the mean (SEM). SEM values were computed by Graphpad Prism from individual mouse averages.

Table 2.1 PCR primers sequences used for genotyping.

Mouse allele	Primer name	Sequence (5'-3')	Product
CreER	Cre347	CCTGGAAAATGCTTCTGTCCG	Amplifies a ~400bp band.
	Cre349	CAGGGTGTTATAAGCAATCCC	
Kras$^{LSL\text{-}G12D}$	Kras1	CTAGCCACCATGGCTTGAGT	Amplifies a ~350bp band.
	Kras2	TCCGAATTCAGTGACTACAGATG	
Trp53^{flox}	Cor-p53int1F	CACAAAAAACAGGTTAAACCCAG	Amplifies a ~370bp mutant and ~290bp wildtype band.
	p53int1R	AGCACATAGGAGGCAGAGAC	
R26R$^{LSL\text{-}YFP}$	R26R-fw	AAAGTCGCTCTGAGTTGTTAT	Amplifies a ~320bp mutant and ~600bp wildtype band.
	R26R-rv	AAGACCGCGAAGAGTTTGTC	
	WT-rv	GGAGCGGGAGAAATGGATATG	
Recombined *Kras*^{G12D}	Web1	GTCTTTCCCCAGCACAGTGC	Amplifies a ~650bp Kras^{G12D} and ~620bp wildtype band.
	Web2	CTCTTGCCTACGCCACCAGCTC	
Recombined *Trp53*	Recomb-p53int1F	CACAAAAAACAGGTTAAACCCAG	Amplifies a ~610bp recombined band.
	Recomb-p53int1R	GAAGACAGAAAAGGGGAGGG	

Chapter 3. Results

3.1 Disease specific survival rates differ significantly between mice with ductal versus acinar cell specific loss of *Trp53* and activation of Kras^{G12D}

To determine how cellular origin affects the initiation and progression of PDAC, I generated mouse models in which a shared set of PDAC-associated mutations were induced in a cell type specific manner. Activation of Kras and loss of wild type *Trp53* are often found in human PDAC (Bailey et al., 2016b; Hruban et al., 1993; Scarpa et al., 1993). Therefore, I chose to model human PDAC development by utilizing Cre-dependent conditional alleles for *Kras* (*Kras$^{LSL\text{-}G12D}$* allele (Tuveson et al., 2004)) and *Trp53* (homozygous *Trp53$^{flox/flox}$* alleles (Marino et al., 2000)) to activate Kras and ablate p53 expression, respectively. To trace the fate of recombined cells and determine recombination specificity, I also included a Cre-dependent yellow fluorescence protein (YFP) reporter allele (*R26R$^{LSL\text{-}YFP}$* allele (Srinivas et al., 2001)). In order to selectively induce Cre-mediated recombination in adult ductal or acinar cells in a temporal manner, I utilized the tamoxifen-inducible transgenic *Sox9CreER* (Font-Burgada et al., 2015; Kopp et al., 2011) or knock-in *Ptf1a^{CreER}* alleles (Pan et al., 2013), respectively. Through cross breeding, I generated *Sox9CreER; Kras$^{LSL\text{-}G12D}$; Trp53$^{flox/flox}$; R26R$^{LSL\text{-}YFP}$* (*Duct:KP^{cKO}*) and *Ptf1a^{CreER}; Kras$^{LSL\text{-}G12D}$; Trp53$^{flox/flox}$; R26R$^{LSL\text{-}YFP}$* (*Acinar:KP^{cKO}*) mice (Figure 3.1A-B). Mice lacking the *Kras* oncogene were used as controls (*Sox9CreER; Trp53$^{flox/flox}$; R26R$^{LSL\text{-}YFP}$* or *Ptf1a^{CreER}; Trp53$^{flox/flox}$; R26R$^{LSL\text{-}YFP}$* mice). To induce recombination, I injected mice with three doses of tamoxifen beginning at three to four weeks of age (Figure 3.2A). This tamoxifen injection protocol resulted in highly efficient YFP labeling of Sox9^{+} ductal or carboxypeptidase A1^{+} (Cpa1^{+}) acinar cells in *Sox9CreER; Trp53$^{flox/flox}$; R26R$^{LSL\text{-}YFP}$* or *Ptf1a^{CreER}; Trp53$^{flox/flox}$; R26R$^{LSL\text{-}YFP}$* mice,

respectively (Figure 3.3A-C and Figure 3.4A-B), four weeks after tamoxifen injection. The labeling induced by the *Sox9CreER* and *Ptf1a*^{CreER} alleles was also highly specific and resulted in less than 2% of Cpa1^{+} acinar cells and less than 0.5% of Sox9^{+} ductal cells being labeled in eight week old *Sox9CreER; Trp53*$^{flox/flox}$*; R26R*$^{LSL\text{-}YFP}$ or *Ptf1a*^{CreER}*; Trp53*$^{flox/flox}$*; R26R*$^{LSL\text{-}YFP}$ mice, respectively (Figure 3.3A).

To examine the effect of activating Kras and ablating *Trp53* on ductal and acinar cells, I injected a cohort of *Duct:KP*^{cKO} (n= 19), and *Acinar:KP*^{cKO} (n= 9) mice with tamoxifen at three to four weeks of age (Figure 3.2A) and monitored the animals until their humane endpoint. *Duct:KP*^{cKO} mice (n=8) died within 10-13 weeks of receiving the tamoxifen injections (Figure 3.2B). Due to the expression and activity of the *Sox9CreER* allele in other organs, such as the oral mucosa, mammary gland, and lung, eleven *Duct:KP*^{cKO} mice reached their humane endpoint due to the presence of masses in these organs. These animals are represented by vertical hashes on the disease specific survival curve and were excluded from further analysis (Figure 3.2B). The remaining eight *Duct:KP*^{cKO} mice reached humane endpoint due to jaundice, weight loss, and/or abdominal distension accompanied by a severe decline in activity (Table 3.1). Upon necropsy, pancreatic tumors were often associated with bile duct blockages resulting in jaundice, as well as metastases in the diaphragm, small bowel penetration accompanied by hemorrhaged blood in the small bowel, and/or large amounts of hemorrhagic or clear ascites fluid (Figure 3.5A-C and Table 3.1). Small nodules of no more than 2mm that were unlikely to affect organ function were also occasionally observed in the liver (Figure 3.5C and Table 3.1; 5/8 *Duct:KP*^{cKO} mice) in *Duct:KP*^{cKO} mice with pancreatic tumors. However, due to Sox9 activity in the liver and the lack of markers to distinguish cholangiocarcinoma and PDAC, the origin of these lesions could not be definitively

identified. Collectively, these observations suggested that the shortened survival time of these eight *Duct:KP^{cKO}* mice (Figure 3.2B) was directly associated with pancreatic tumorigenesis.

Acinar:KP^{cKO} mice reached humane endpoint at 15-23 weeks post tamoxifen injection (Figure 3.2C). Similar to *Duct:KP^{cKO}* mice, these mice also developed jaundice, abdominal distensions, and/or significant weight loss (n= 8, Table 3.1). Upon necropsy, pancreatic tumors were associated with obstruction of the common bile duct, accumulation of hemorrhagic or clear ascites fluid, or penetration of the small bowel (Figure 3.5A-C, and Table 3.1). The lack of tumors in other organs, as well as the prominence of tumors in the pancreas, indicated that these mice also reached humane endpoint due to pancreatic tumorigenesis. This suggested that loss of *Trp53* in the presence of activated Kras^{G12D} induced tumorigenesis from both ductal and acinar cell. However, *Acinar:KP^{cKO}* mice had a median disease specific survival rate that was seven weeks longer than *Duct:KP^{cKO}* mice ($p < 0.0001$) and did not have any signs of distant metastases (Table 3.1), suggesting that cell-of-origin can affect tumor development and/or phenotype.

3.2 Loss of *Trp53* in Kras^{G12D}-expressing ductal or acinar cells induces PDAC

To determine whether differences in the survival outcomes of *Duct:KP^{cKO}* and *Acinar:KP^{cKO}* mice were due to different types of tumors forming in each model, I extensively characterized the tumors formed by ductal or acinar cells. The pancreata of both *Duct:KP^{cKO}* and *Acinar:KP^{cKO}* mice had solid tumor nodules, ranging from small, distinct nodes to complete displacement of normal parenchyma by tumor (Figure 3.5A, Figure 3.6A and data not shown). Hematoxylin and eosin staining confirmed that these tumors were

comprised of ductal or glandular structures arranged in a haphazard pattern (Figure 3.6B), consistent with PDAC. Furthermore, tumors from *Acinar:KP^{cKO}* mice showed additional tumor phenotypes, ones resembling cysts ("cystic") or precursor lesions ("precursor-like") (Figure 3.7A-B and Table 3.1). Histologically, the majority of the tumors were epithelial, and mostly of moderate or poor differentiation status. However, a range of tumor grades from well to poorly differentiated was observed in both mouse models (Figure 3.8A). To confirm these tumors were ductal in nature, I performed immunohistochemistry stains to detect ductal markers, including cytokeratin 19 (CK19), Sox9, and Hnf1b. These stainings revealed that all tumors from the *Duct:KP^{cKO}* and *Acinar:KP^{cKO}* mice were strongly positive for ductal markers including CK19, Sox9 and Hnf1b (Figure 3.8B, Figure 3.9 and Table 3.1). To examine the lineage origin of these tumors, I performed immunohistochemistry staining to detect the lineage reporter protein, YFP. Consistent with an origin from ductal or acinar cells, tumors in *Duct:KP^{cKO}* and *Acinar:KP^{cKO}* mice, respectively, were YFP positive (Figure 3.8B). In addition, I assessed recombination of the *Kras$^{LSL\text{-}G12D}$* and *Trp53^{flox}* alleles by PCR on whole pancreas sections, which included non-cancerous tissue. I observed recombination of both the *Kras$^{LSL\text{-}G12D}$* and *Trp53^{flox}* alleles, suggesting that the tamoxifen induced recombination of these alleles was successful (Figure 3.10A). Consistent with the recombination results, immunohistochemistry against p53 confirmed that p53 was absent in all tumor epithelial tissue analyzed from both *Acinar:KP^{cKO}* and *Duct:KP^{cKO}* mouse models (Figure 3.10B-C). Together, these data indicated that both Kras^{G12D} expressing acinar and ductal cells contributed to PDAC in the absence of p53.

3.3 Similar tumor burden is present in *Duct:KP^{cKO}* and *Acinar:KP^{cKO}* mouse models, but appears earlier in *Duct:KP^{cKO}* mice

To begin to identify factors that contribute to the differential survival outcomes of *Duct:KP^{cKO}* and *Acinar:KP^{cKO}* mice, I examined whether tumor size, number or location differed between these two mouse lines at the humane endpoint. I estimated the amount of overall tumor burden in each mouse through the use of whole section imaging to quantify the pancreatic section area that was displaced by tumor. In parallel, I also quantified the sizes of individual tumors by measuring the maximal cross-sectional diameter. Although the overall pancreatic area displaced by tumor varied from animal to animal, the average tumor burden was similar between *Duct:KP^{cKO}* and *Acinar:KP^{cKO}* mice (Figure 3.11A and Table 3.1). In addition, I found that the numbers of tumors that developed and the sizes of these tumors in *Duct:KP^{cKO}* and *Acinar:KP^{cKO}* mice were not significantly different (Figure 3.11B-C). Furthermore, I also examined whether preferential location of tumors near the common/main duct in the pancreatic head and induction of cholestasis could explain the survival differences in *Duct:KP^{cKO}* or *Acinar:KP^{cKO}* mice. Our necropsy analysis indicated that bile duct constriction/obstruction and jaundice was observed in certain cases and most likely resulted in reduced survival times for some animals, however, the frequency of these events in *Duct:KP^{cKO}* and *Acinar:KP^{cKO}* mice were similar (Table 3.1). Consistently, our quantification of tumor location in the pancreatic head, body and tail showed that tumors from both acinar and ductal cells were similarly biased to the pancreatic head/body (Figure 3.11D). Together these data suggested that differences in survival between *Duct:KP^{cKO}* and *Acinar:KP^{cKO}* mice cannot solely be attributed to tumor burden or location. However, one striking difference between the two models was that the maximal tumor burden occurred

earlier in *Duct:KP^{cKO}* compared to *Acinar:KP^{cKO}* mice (Figure 3.11A), which suggested that tumor initiation and/or development may be the cause of the survival difference.

3.4 *Duct:KP^{cKO}* mice develop tumors earlier than *Acinar:KP^{cKO}* mice.

To study early tumor initiation in *Duct:KP^{cKO}* and *Acinar:KP^{cKO}* mice, I injected mice of both genotypes plus controls at three to four weeks of age with tamoxifen and then collected the pancreata from *Duct:KP^{cKO}* and *Acinar:KP^{cKO}* mice at time points prior to the median survival time of *Duct:KP^{cKO}* and *Acinar:KP^{cKO}* mouse lines (specifically, between 2 to 8 or 4 to 16 weeks post injection, respectively) (Figure 3.12A). Using these earlier timepoints, I next asked whether ductal cell derived tumors were initiated earlier than those from acinar cells. To do this, I stained pancreatic sections from the early timepoints with H&E and then quantified the numbers and sizes of the tumors. These analyses revealed considerable differences in the timing of tumor development in *Duct:KP^{cKO}* compared to *Acinar:KP^{cKO}* mice. In two *Duct:KP^{cKO}* mice, a small number of focal tumors less than 1mm in size were observed as early as four weeks after tamoxifen injection and the tumors steadily increased in size and number over the course of the timepoint analysis (Figure 3.13A-B). In contrast, no tumors were observed in *Acinar:KP^{cKO}* mice until eight weeks post tamoxifen injection (Figure 3.12B-C, arrowheads and Figure 3.13A-B). No obvious patterns of growth could be identified following tumor initiation at 8 weeks post tamoxifen injection, as there appeared to be extensive variation in both tumor size and number (Figure 3.13A-B). Taken together, these data suggest that differences in PDAC initiation resulted in the survival difference between *Duct:KP^{cKO}* and *Acinar:KP^{cKO}* mice. In support of this, the four week delay in tumor initiation in *Acinar:KP^{cKO}* mice approximately matched the difference in time (34 days) between the first animals of each model succumbing to the disease (Figure 3.2B).

In sum, tumors in *Duct:KP^{cKO}* mice were initiated at earlier time points, which I hypothesize resulted in the extended survival of mice with acinar cell derived tumors.

To further test whether differences in PDAC initiation and not tumor growth explained the distinct survival outcomes of each mouse model, I examined the rates of proliferation and apoptosis. To do this, I stained representative tumor sections at various timepoints and of various sizes for Ki67 (a proliferation marker) and cleaved caspase 3 (an apoptosis marker). I found that the extent of Ki67 and cleaved caspase3 positivity did not differ in tumors from either mouse line (Figure 3.14A-C). This suggests that the accelerated tumor development in the *Duct:KP^{cKO}* mouse model is a result of differences in initiation and not accelerated tumor growth in *Duct:KP^{cKO}* mice.

3.5 High-grade mPanINs are found in both models, but *Duct:KP^{cKO}* mice lack low-grade mPanINs

Since the initiation of PDAC from ductal cells appeared to be much earlier than initiation from acinar cells, I next examined whether differential tumor initiation was a result of differences in precursor lesion initiation or progression. Development of pancreatic cancer is associated with the formation of precancerous lesions, called pancreatic intraepithelial neoplasia (PanIN) (Brat et al., 1998). PanINs are thought to go through a low-grade to high-grade progression scheme with the high-grade lesions, or *carcinoma in situ*, acquiring loss of tumor suppressors, such as *Trp53* (Figure 1.1) (DiGiuseppe et al., 1994; Wilentz et al., 2000; Yamano et al., 2000). To quantify potential differences in mPanIN initiation or progression, I quantified the number of mPanINs present per representative section at two, four, six, and eight weeks after tamoxifen injection for *Duct:KP^{cKO}* mice and at four, six, eight, twelve and sixteen weeks post-injection for *Acinar:KP^{cKO}* mice. All abnormal duct-like glands with a

lumen were classified as acinar-to-ductal metaplasia, mPanIN1, mPanIN2, or mPanIN3 (see methods for more details) (Figure 3.15A-B). To strictly quantify precancerous lesions, glandular structures directly associated with PDAC were excluded from this analysis. The number and grade of mPanINs in each group at the indicated time points were then graphed as a circle representative of the average number of mPanINs (Figure 3.16A). Because the largest number of mPanIN present per section per *Acinar:KP^{cKO}* mouse was the mPanIN1 group at sixteen weeks post injection (approximately 200), this sample was set to 1 as the point of comparison (Figure 3.16A, bottom right-hand corner). I observed low-grade mPanIN as early as four weeks post injection in *Acinar:KP^{cKO}* mice and these numbers increased with time. Simultaneously, I observed high-grade mPanIN in *Acinar:KP^{cKO}* mice beginning at four weeks post injection that then became more numerous at later ages with over twenty mPanIN3 lesions per section per mouse. In addition to finding mPanIN of all grades, *Acinar:KP^{cKO}* mice also tended to display a much greater capacity to develop ductal metaplasia, as demonstrated by the higher ratio of abnormal (non-tumor) metaplastic ductal area per total pancreatic area (Figure 3.16B). In spite of the abundance of precursor lesions, *Acinar:KP^{cKO}* mice did not develop significantly more PDAC than *Duct:KP^{cKO}* mice (Figure 3.11B-C and Figure 3.13A). This suggested that although acinar cells readily transition into mPanIN lesions, few of these hyperplastic/metaplastic ducts ever become neoplastic.

Kopp et al. (2012) and others have previously shown that Kras^{G12D}-expressing ductal cells can generate small numbers of low-grade PanIN lesions (at most 10 mPanINs per mouse (Kopp et al., 2012; Ray et al., 2011)). However, in the absence of *Trp53*, ductal cells did not form any low-grade mPanIN and primarily formed small numbers of high-grade mPanIN3 lesions, at a frequency of approximately one per section per mouse by 4 weeks

post tamoxifen injection (Figure 3.15A-B and Figure 3.16A-B). This suggests that unlike *Acinar:KP^{cKO}* mice, *Duct:KP^{cKO}* mice expressing Kras^{G12D} in the absence of p53 rapidly initiated carcinomas without simultaneously developing low-grade precursor lesions. Because oncogenic Kras alone frequently induces low-grade mPanINs from acinar cells, I next examined whether the presence of low-grade mPanIN in the acinar cell-specific model was due to inefficient recombination of the *Trp53^{flox}* alleles (Figure 3.17A). Recombination of the *R26R$^{LSL-YFP}$* reporter allele is not always indicative of successful recombination at the *Trp53* loci due to differences in genetic context (Coppoolse et al., 2005; Vooijs et al., 2001; Zheng et al., 2000), therefore I immunohistochemically stained for p53 expression to use as a surrogate marker for *Trp53$^{flox/flox}$* allele recombination. These analyses revealed that carcinoma-in-situ (mPanIN3) from both *Acinar:KP^{cKO}* and *Duct:KP^{cKO}* mice, like PDAC (Figure 3.10B), did not express p53 (Figure 3.17B). Protein p53 expression was also lost in some low-grade acinar cell derived mPanINs, which suggests that low-grade mPanIN can form from acinar cells in the absence of p53. However, low-grade PanIN were more variable in their p53 positivity suggesting that some may also arise as a result of inefficient recombination at the *Trp53* locus (Figure 3.17C). Together, these data suggest that the grade of mPanINs generated prior to PDAC initiation from Kras^{G12D}-expressing acinar cells may be distinct from that of ductal cells in the absence of p53 (Figure 3.17C). In sum, these results were congruent with a previous finding reporting that acinar cells expressing Kras^{G12D} and single copy mutant *Trp53* continued to form low-grade mPanIN lesions (Bailey et al., 2016a), like those described here (Figure 3.16A).

Unlike low-grade mPanIN, high-grade mPanINs were observed in *Duct:KP^{cKO}* mice by four weeks post tamoxifen injection. Furthermore, the quantity of high-grade lesions

present were comparable to numbers found in *Acinar:KP^{cKO}* mice at the same time point. Although mPanIN3 lesions were present at similar numbers in each mouse model, at four weeks post-injection, pancreata from *Duct:KP^{cKO}* mice already contained invasive PDAC (Figure 3.13A). The number of mPanIN3 lesions in *Duct:KP^{cKO}* remained similar over the next four weeks and tumors accumulated rapidly over the same time frame (Figure 3.13A). This suggested that as mPanIN3 lesions from ductal cells were induced, they quickly became invasive, which resulted in the earlier demise of *Duct:KP^{cKO}* mice (Figure 3.13A and Figure 3.2B). However, in *Acinar:KP^{cKO}* mice, the number of mPanIN3 lesions increased and accumulated from 4 to 16 weeks post tamoxifen, but the number of tumors did not increase until eight weeks post tamoxifen injection (Figure 3.16A). This suggested that although both mouse models have mPanIN3 lesions, the tumorigenic potential of the ductal-cell-derived lesions was greater than those derived from acinar cells. Thus, the reduced survival time of *Duct:KP^{cKO}* mice compared to *Acinar:KP^{cKO}* mice may be due to the increased propensity of Kras^{G12D}-expressing ductal cells to induce mPanIN3 and convert to PDAC in the absence of p53.

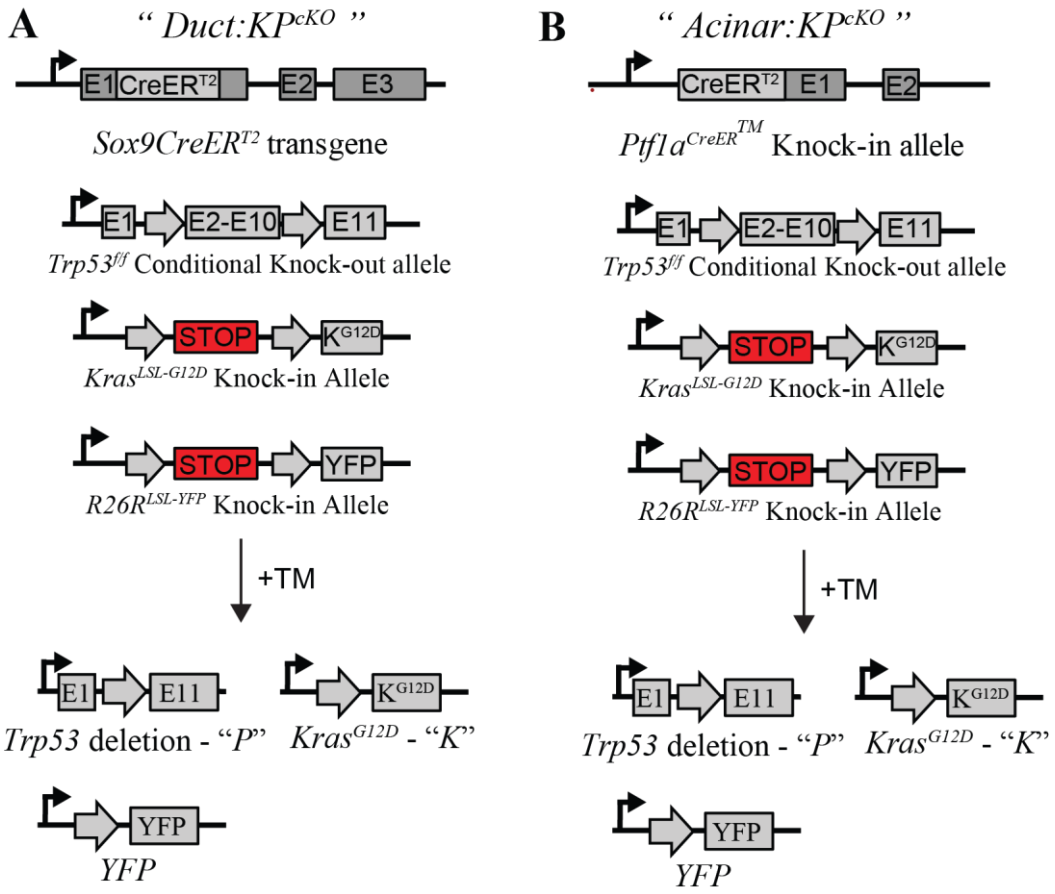

Figure 3.1 Schematic describing the alleles utilized to generate the *Sox9CreER*; *Kras*$^{LSL\text{-}G12D}$; *Trp53*$^{flox/flox}$; *R26R*$^{LSL\text{-}YFP}$ and *Ptf1a*^{CreER}; *Kras*$^{LSL\text{-}G12D}$; *Trp53*$^{flox/flox}$; *R26R*$^{LSL\text{-}YFP}$ mouse models used in this study.

Figure 3.1 Identical genetic mutations (oncogenic $Kras^{G12D}$ expression and *Trp53* deletion) were targeted to different cell types of the pancreas. Tamoxifen (TM) injection induces nuclear localization of the CreER protein and results in Cre-mediated DNA recombination and expression of oncogenic $Kras^{G12D}$ from the $Kras^{LSL\text{-}G12D}$ allele ("*K*"), deletion of exons 2-10 from the $Trp53^{flox}$ allele ("P^{cKO}"), resulting in loss of p53 expression. **A**) The expression of the CreER gene was driven by the *Sox9* promoter in the ductal cell specific model (abbreviated as "$Duct{:}KP^{cKO}$"). **B**) The expression of the *CreER* gene was driven by the *Ptf1a* promoter in the acinar cell specific model (abbreviated as "$Acinar{:}KP^{cKO}$").

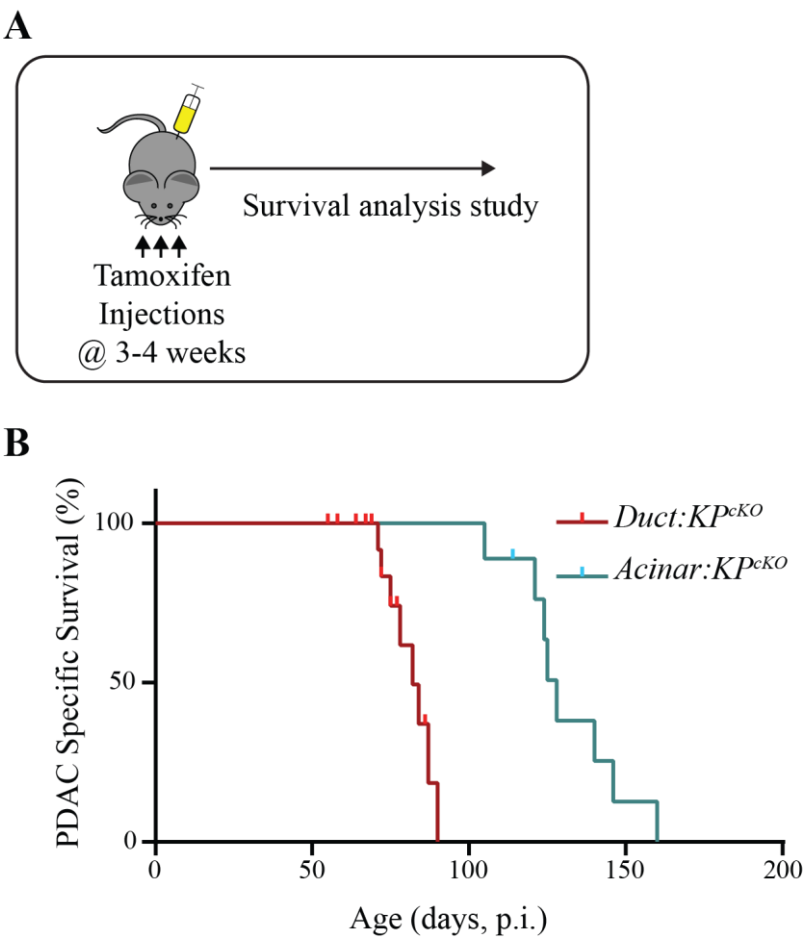

Figure 3.2 The disease specific survival of mice in which oncogenic *Kras*^{G12D} is expressed and *Trp53* is ablated in a ductal or acinar cell specific manner differs.

A) *Duct:KP*^{cKO} (n= 19) and *Acinar:KP*^{cKO} (n= 9) mice were injected three times on alternating days with tamoxifen (TM) beginning at three to four weeks of age. The mice were monitored until they reached their humane endpoint to determine survival duration. **B**) The median disease specific survival of *Duct:KP*^{cKO} mice was 82 days, which was significantly shorter than the *Acinar:KP*^{cKO} mice at 128 days ($p<0.0001$). Mice euthanized for non-pancreatic reasons were censored (hash marks). p.i., post tamoxifen injection.

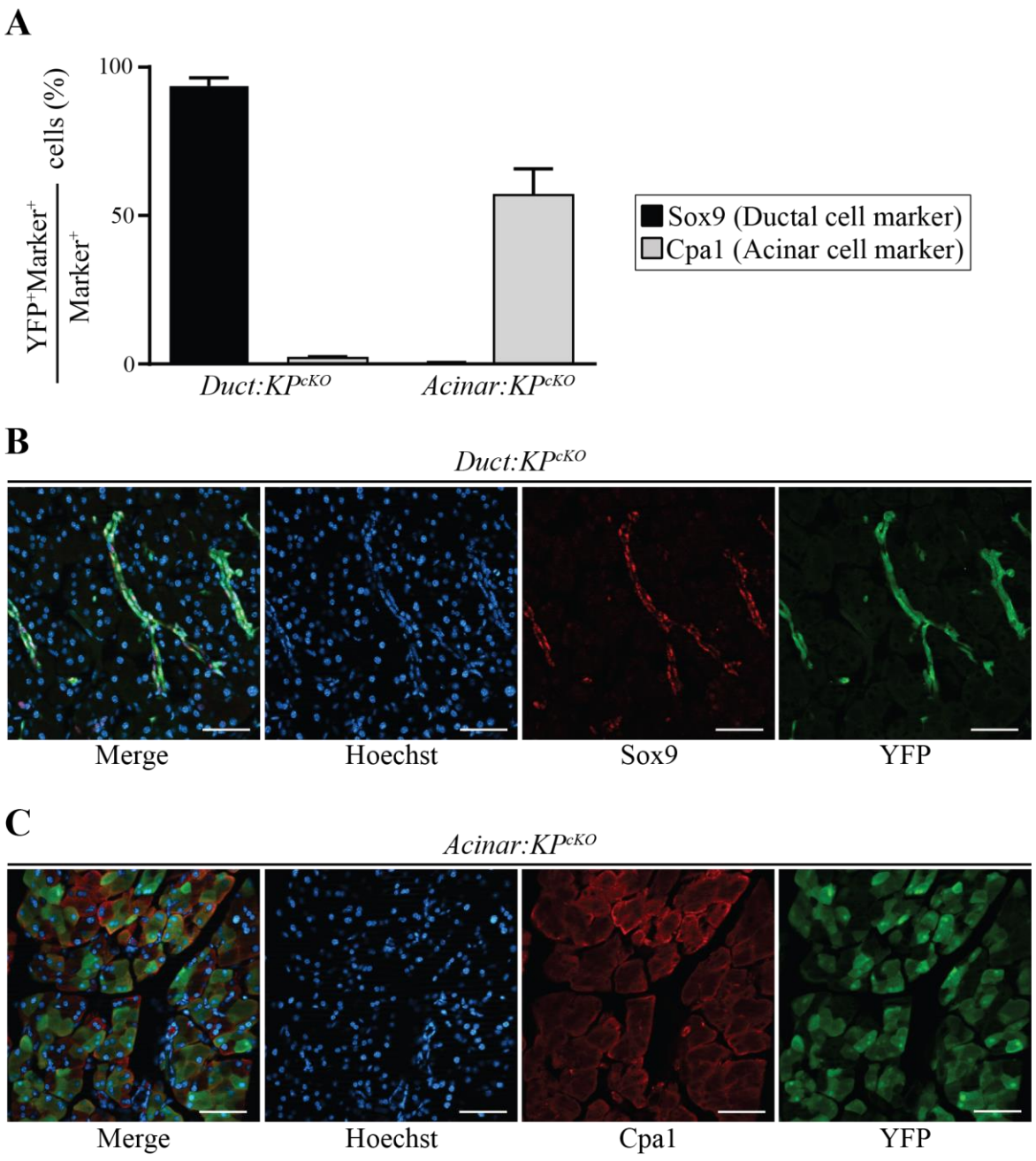

Figure 3.3 *Sox9CreER* and *Ptf1a*^{CreER} alleles induces highly cell type specific chromosomal recombination in ductal and acinar cells, respectively.

Figure 3.3 The specificity of both mouse lines was assessed using immunofluorescence to detect colocalization of the lineage label YFP with either ductal or acinar cell specific markers such as Sox9 or Cpa1, respectively. **A**) Recombination was found to be highly specific, with less than 2% of $Cpa1^{+}$ acinar cells and less than 0.5% of $Sox9^{+}$ ductal cells being labeled in *Sox9CreER; Trp53$^{flox/flox}$; R26R$^{LSL\text{-}YFP}$* or *Ptf1a^{CreER}; Trp53$^{flox/flox}$; R26R$^{LSL\text{-}YFP}$* mice, respectively. Furthermore, recombination of the *R26R$^{LSL\text{-}YFP}$* allele was also found to be highly efficient, 94% ductal cell recombination for *Sox9CreER; Trp53$^{flox/flox}$*; *R26R$^{LSL\text{-}YFP}$* mice and 60% acinar cell recombination for *Ptf1a^{CreER}; Trp53$^{flox/flox}$; R26R$^{LSL\text{-}YFP}$* mice Nine sections were analyzed from three animals per model to determine co-localization of YFP with Sox9 in *Sox9CreER; Trp53$^{flox/flox}$; R26R$^{LSL\text{-}YFP}$* pancreata, or YFP with CPA1 in *Ptf1a^{CreER}; Trp53$^{flox/flox}$; R26R$^{LSL\text{-}YFP}$* pancreata. **A**) *Sox9CreER; Trp53$^{flox/flox}$; R26R$^{LSL\text{-}YFP}$* mice showed highly efficient recombination in ductal cells (93.6%) and minimal off-target recombination in acinar cells (2.0%). Similarly, *Ptf1a^{CreER}; Trp53$^{flox/flox}$; R26R$^{LSL\text{-}YFP}$* mice showed efficient recombination in acinar cells (56.9%) and minimal off-target recombination in ductal cells (0.4%). **B and C**) Co-immunofluorescence staining for Sox9 and YFP in the ductal cell specific model and Cpa1 and YFP in the acinar cell specific model demonstrated target cell type specificity. Scale: 100 μm (B-C).

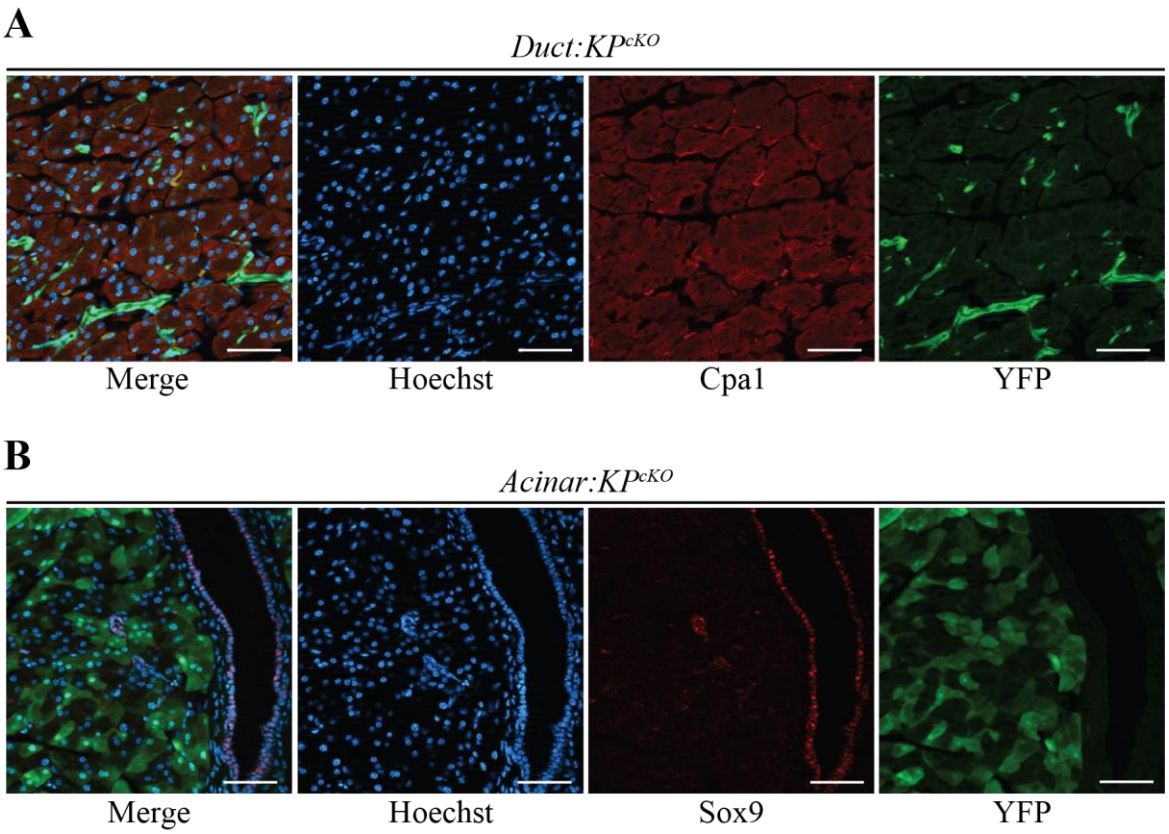

Figure 3.4 *Sox9CreER* and *Ptf1a*^{CreER} alleles exhibit little to no off-target recombination. Six sections were analyzed from two animals per model to determine co-localization of YFP with CPA in *Sox9CreER; Trp53*$^{flox/flox}$*; R26R*$^{LSL\text{-}YFP}$ pancreata, or YFP with Sox9 in *Ptf1a*^{CreER}*; Trp53*$^{flox/flox}$*; R26R*$^{LSL\text{-}YFP}$ pancreata. Co-immunofluorescence staining for **A**) Cpa1 and YFP in the ductal cell specific model and **B**) Sox9 and YFP in the acinar cell specific model, demonstrated minimal off-target recombination. Scale: 100 μm (A-B).

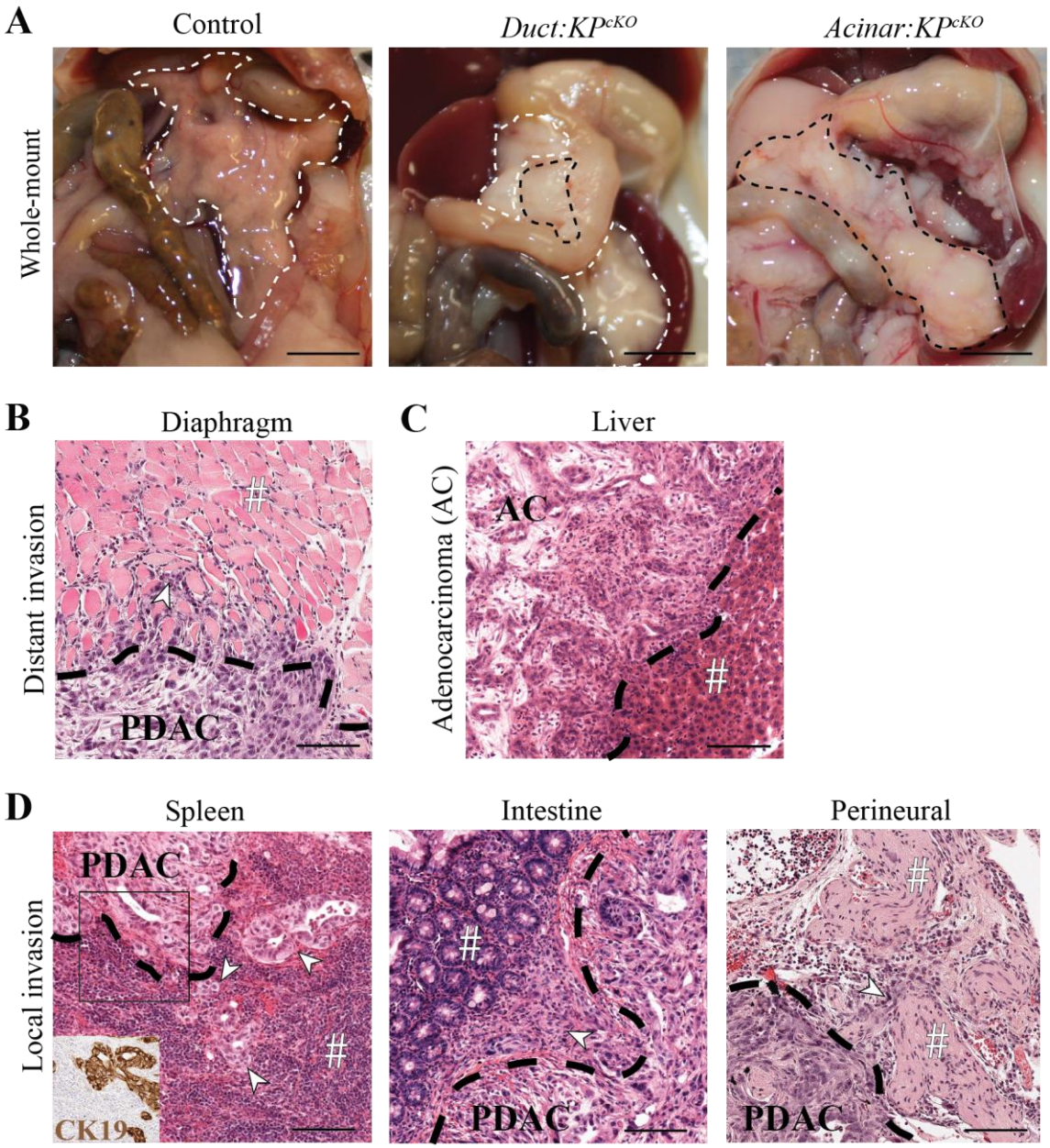

Figure 3.5 *Duct:KP^{cKO}* and *Acinar:KP^{cKO}* mice develop distally and locally invasive tumors.

Figure 3.5 A) Representative gross pathological photographs of mouse pancreata from *Sox9CreER*; *Trp53*$^{flox/flox}$; *R26R*$^{LSL\text{-}YFP}$ mice (Control), *Duct:KP*^{cKO} mice, and *Acinar:KP*^{cKO} mice. Tumors have a dull, and nodular appearance compared to normal pancreatic parenchyma, which has a uniform color and consistency. White or black dashed lines outline either normal parenchyma or tumors, respectively. **B**) Tumor has been shown to invade into distant tissues, such as the diaphragm. **C**) Small adenocarcinomas were occasionally found in the livers of *Duct:KP*^{cKO} mice. However, liver Sox9 activity precluded metastasis analysis in this organ, as there are no known markers to distinguish cholangiocarcinoma from metastatic PDAC. Invasion into nearby tissues such as the **D**) spleen, intestine or nerves was frequently observed. Boxed area in D) spleen is shown in the inset, stained with CK19 from a nearby section. The approximate border between PDAC and the tissue being invaded into is demarcated by a black dashed line. The location of normal tissue is indicated by "#" and tumor cells are marked by arrowheads. Scale bars: 5 mm (A), 100 µm (B-C).

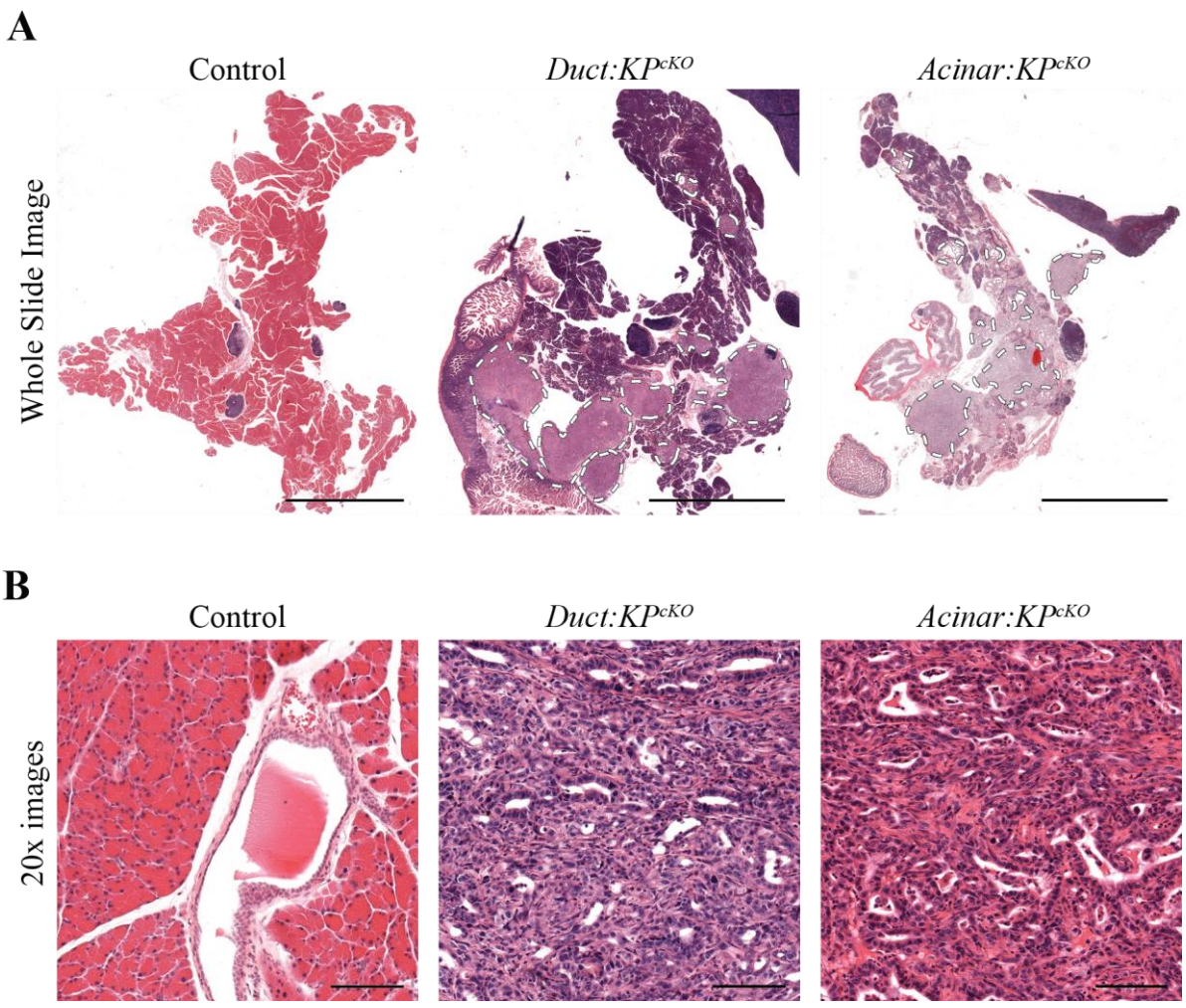

Figure 3.6 *Duct:KP^{cKO}* and *Acinar:KP^{cKO}* mice develop morphologically similar tumors that exhibit haphazard ductules interspersed in stroma.

A) Representative whole slide images of H&E stained *Sox9CreER; Trp53$^{flox/flox}$; R26R$^{LSL-YFP}$* (Control), *Duct:KP^{cKO}* and *Acinar:KP^{cKO}* pancreata. Tumors are outlined in dashed lines. The pancreatic tail and head are located at the top and bottom of the image, respectively. **B**) H&E staining of pancreata from Control, *Duct:KP^{cKO}* and *Acinar:KP^{cKO}* mice show that both *Duct:KP^{cKO}* and *Acinar:KP^{cKO}* develop tumors more similar to ductal cells than acinar cells and possess morphologies typical of PDAC. Scale bars: 5 mm in A, 100 μm in B.

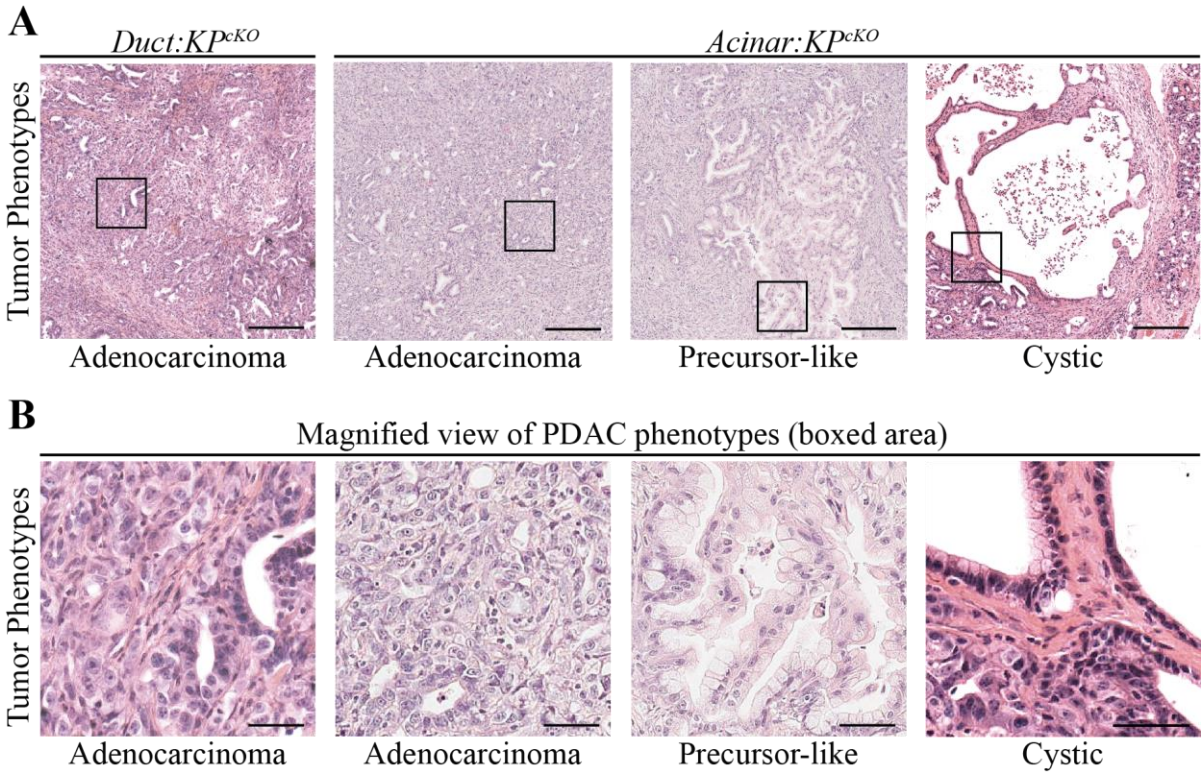

Figure 3.7. *Acinar:KP^{cKO}* tumors a display precursor-like or cystic tumor phenotype in addition to the typical ductal epithelial phenotype of ductal adenocarcinoma.

Whole pancreatic sections were scanned and analyzed for the presence of different tumor phenotypes at humane endpoint. **A**) Common to both models were the adenocarcinoma phenotype, shown with an abundance of haphazard ductules interspersed within some stroma. The precursor-like phenotype was defined as tumors with a significant number of columnar, hypermucinous ductules resembling those from low-grade mPanIN lesions (mPanIN1 or mPanIN2). The cystic phenotype was defined as tumors with large cystic cavities lined with a single layer of cuboidal or columnar epithelium that may be somewhat mucinous. **B**) Magnified view of boxed area shown in A) of observed PDAC phenotypes.

Scale: 200 μm (A) and 50 μm (B).

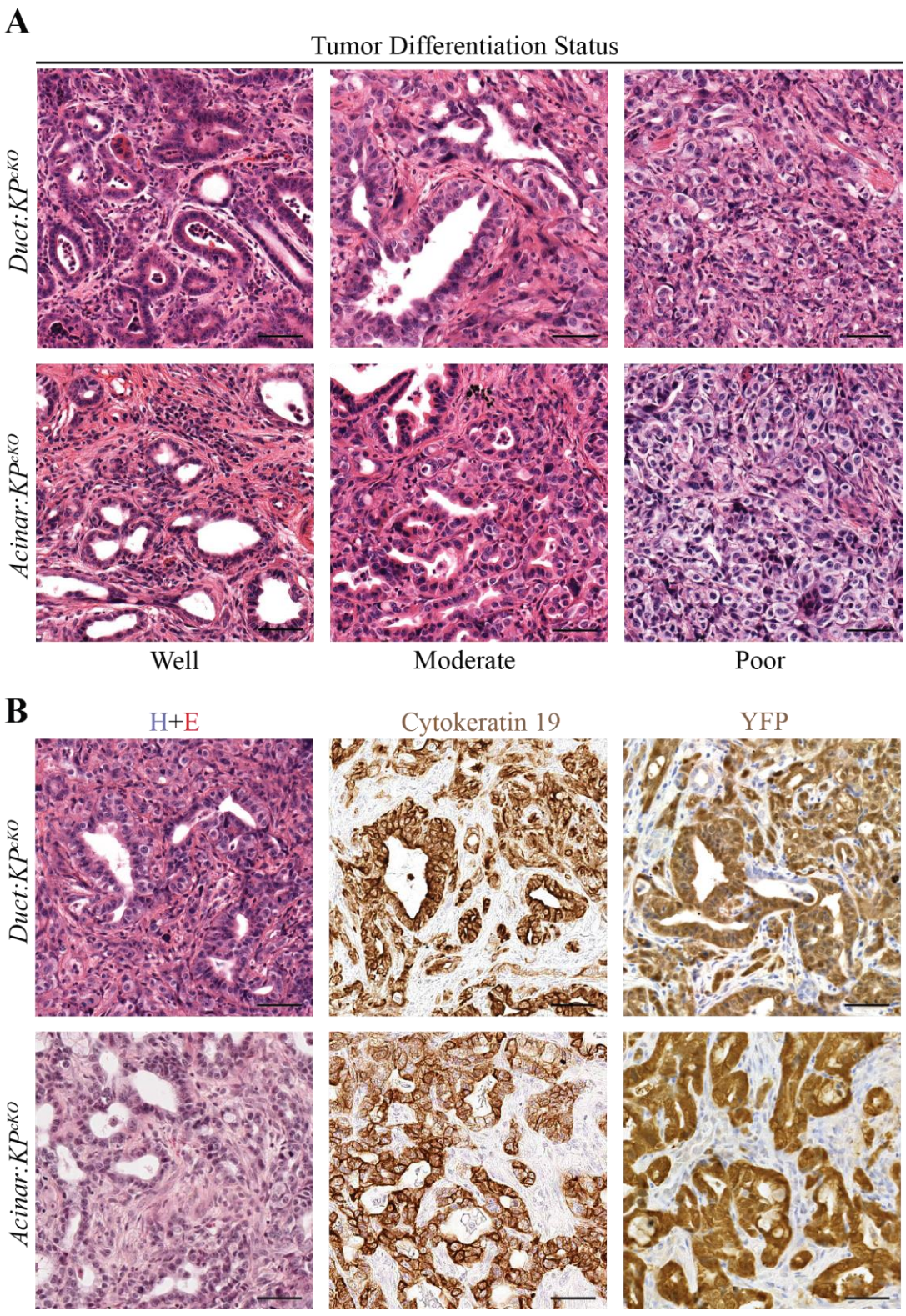

Figure 3.8 *Duct:KP^{cKO}* and *Acinar:KP^{cKO}* develop PDAC tumors of varying differentiation status.

Figure 3.8 A) Differentiation status was evaluated based upon how glandular and structured the PDAC appeared. The differentiation status ranged from well to poorly differentiated and different classifications could be observed in the same tumor. Every classification from well to poorly differentiated was observed in both *Duct:KP*^{cKO} and *Acinar:KP*^{cKO} mouse models. **B**) Immunohistochemical staining for CK19 and YFP verified the duct-like nature and cellular origin, respectively, of PDAC formed in *Duct:KP*^{cKO} and *Acinar:KP*^{cKO} mice. Scale bars: 50 μm (A-B).

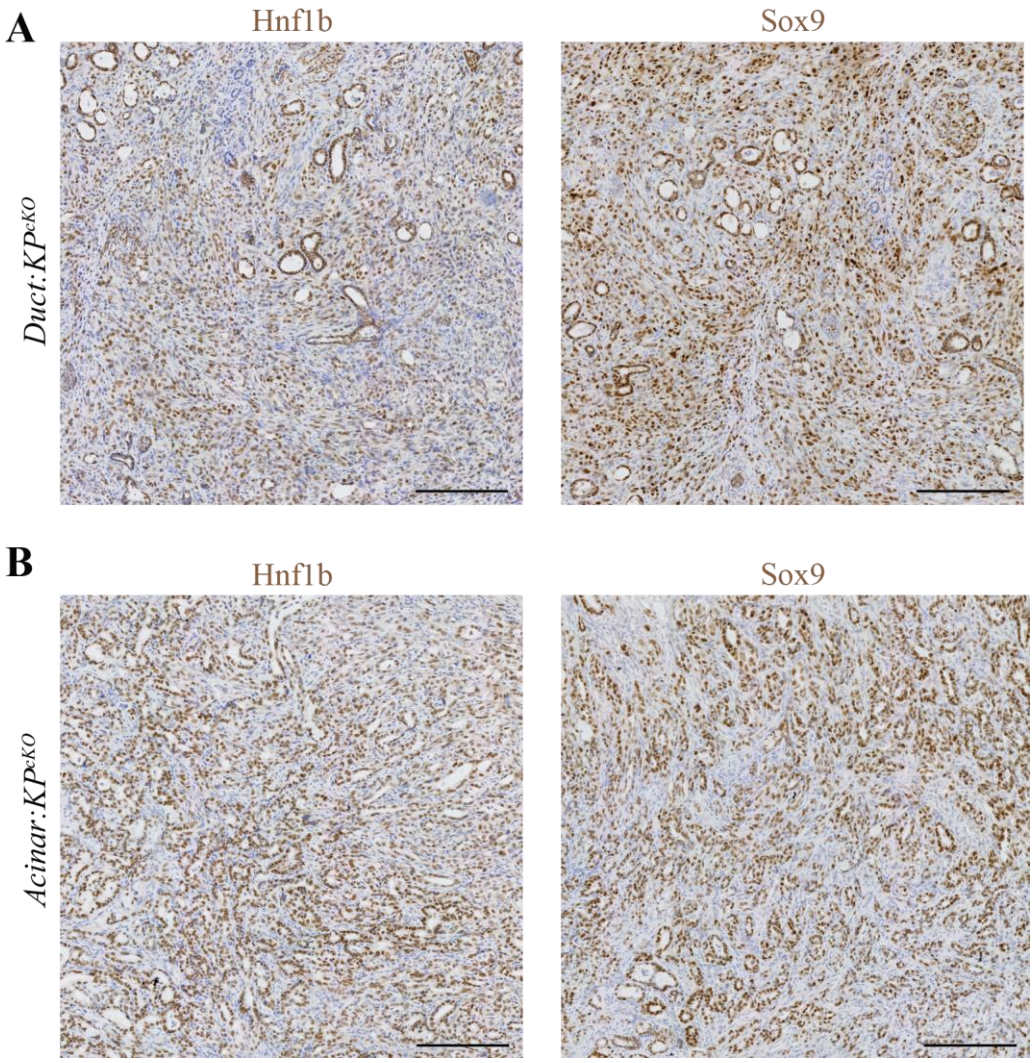

Figure 3.9 Wide field-of-view images from representative tumors of *Duct:KP^{cKO}* and *Acinar:KP^{cKO}* mice.

Both *Duct:KP^{cKO}* and *Acinar:KP^{cKO}* mouse lines seen in **A**) and **B**), respectively, show ductal marker (Hnf1b and Sox9) expression in tumor epithelial cells. Note that the stroma is negative for ductal markers and is interspersed amongst the haphazard PDAC ductules. Scale: 200 µm (A-B).

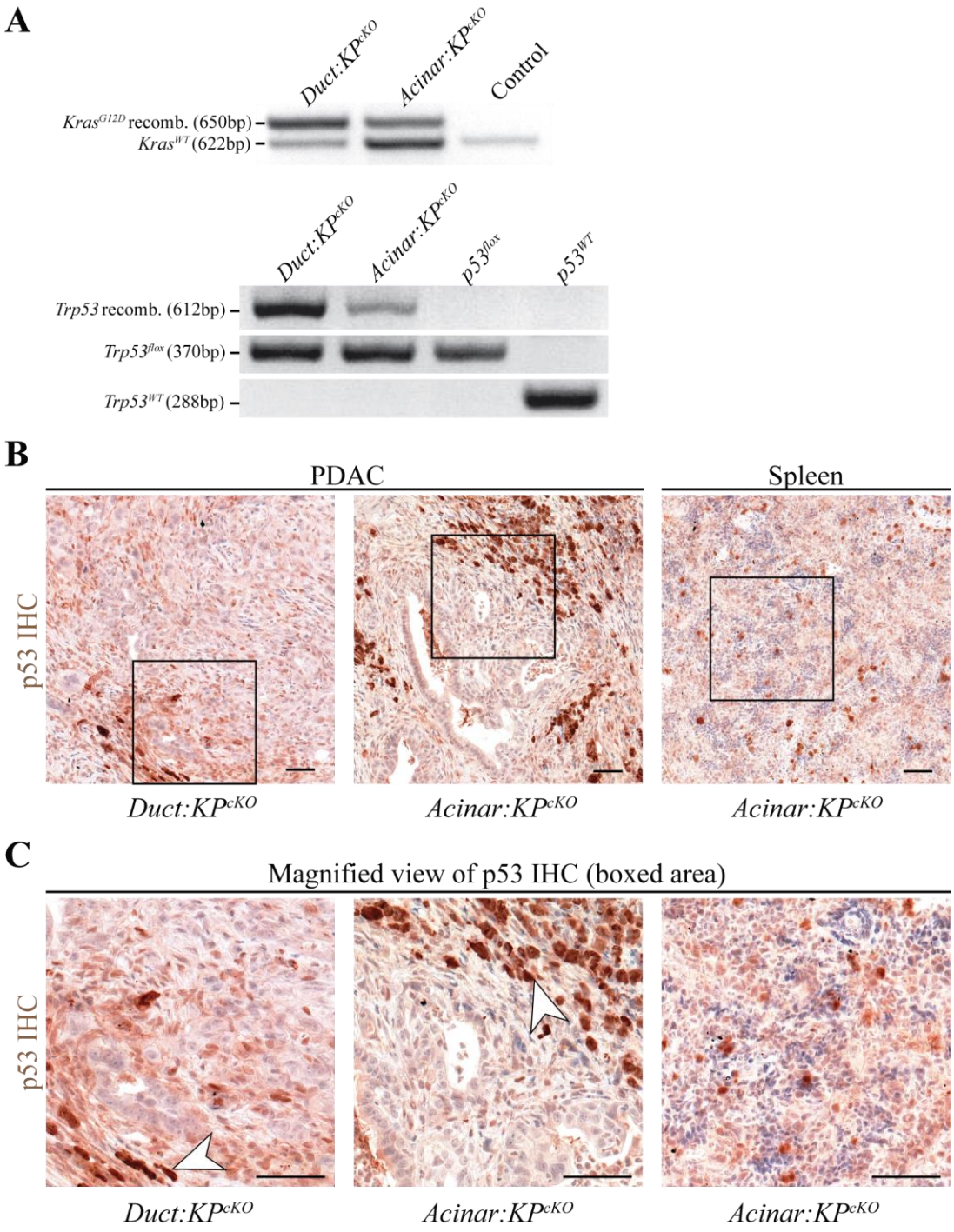

Figure 3.10 Confirmation of p53 ablation by PCR and immunohistochemistry.

Figure 3.10 A) Whole pancreas formalin fixed paraffin embedded (FFPE) sections, including normal stroma, parenchyma and tumors from *Duct:KP^{cKO}* and *Acinar:KP^{cKO}* mouse models were deparaffinzed, digested and genotyped to confirm, in a non-quantitative manner, recombination of the *Kras$^{LSL\text{-}G12D/+}$* and *Trp53$^{flox/flox}$* alleles. *Trp53$^{flox/flox}$* mice were not exposed to tamoxifen and therefore no recombination was observed, as expected. Wild-type pancreata were used for the *Kras$^{WT/WT}$* and *Trp53$^{WT/WT}$* controls. **B**) Immunohistochemistry against p53 was carried out on PDAC and spleens from both *Duct:KP^{cKO}* and *Acinar:KP^{cKO}* mouse models. Tumor cells from both *Duct:KP^{cKO}* and *Acinar:KP^{cKO}* mice were found to have lost p53 expression in almost all cases, with rare exceptions. However, p53 expressing cells were observed in the stroma, as well as in the splenic white pulp, and were used as positive control (representative image from *Acinar:KP^{cKO}* mouse line shown). **C**) Magnified view of boxed areas in B), showing a lack of p53 expression in tumor epithelial cells, but p53 positivity from cells in the stroma (arrows). Scale bars: 50 μm (B-C).

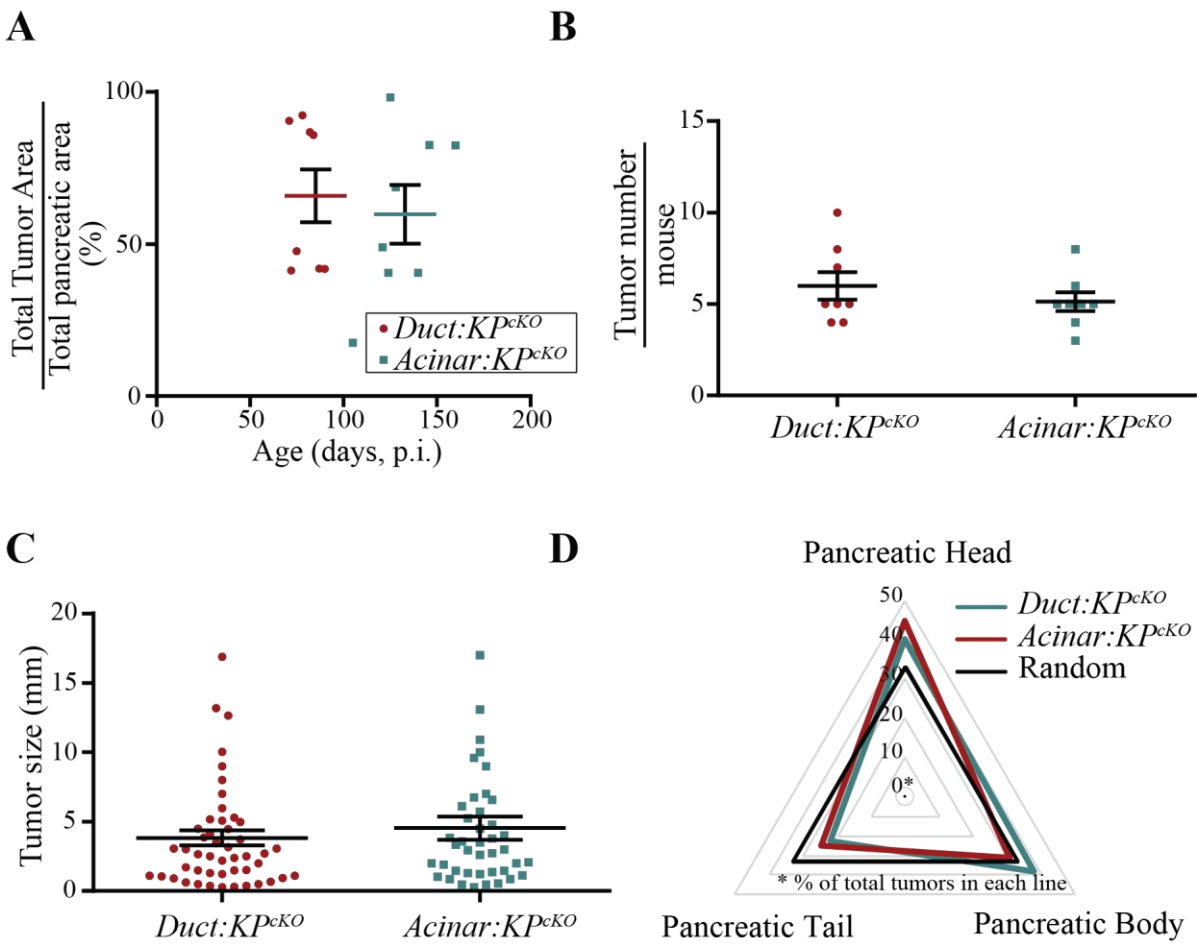

Figure 3.11 PDAC tumors from both *Duct:KP^{cKO}* and *Acinar:KP^{cKO}* models show similar tumor burden, sizes, numbers, and subsite distribution, but ductal cell derived PDAC is observed earlier.

Figure 3.11 A) Quantification of tumor burden at the humane endpoint (survival cohort) between *Duct:KP^{cKO}* and *Acinar:KP^{cKO}* mice revealed that both mouse models have similar amounts of pancreatic area displaced by tumor area (y-axis, 65.9 ± 8.7%, 59.9 ± 9.7%, respectively and p=0.43). However, tumors were observed earlier in *Duct:KP^{cKO}* (x-axis, median 82 days post tamoxifen injection) compared to *Acinar:KP^{cKO}* mice (median 128 days post tamoxifen injection). **B**) Quantification of the number of tumors present per mouse at the humane endpoints for the *Duct:KP^{cKO}* and *Acinar:KP^{cKO}* mouse survival cohort (6.0 ± 0.8, 5.1 ± 0.5, respectively and p=0.58). **C**) Quantification of the largest cross-sectional diameter (tumor size) for each tumor found in *Duct:KP^{cKO}* and *Acinar:KP^{cKO}* mice 3.8 ± 0.5mm, 4.5 ± 0.8mm, respectively, and p=0.63). **D**) Radar diagram indicating the percentage of tumors found in pancreatic head, tail, or body for the *Duct:KP^{cKO}* and *Acinar:KP^{cKO}* survival mouse cohort. The black line indicates what would be expected if tumors were randomly initiated in the head, tail and body (33% per subsite). Similar to human tumors, tumors in *Duct:KP^{cKO}* and *Acinar:KP^{cKO}* mice are more likely to be found near the head of the pancreas.

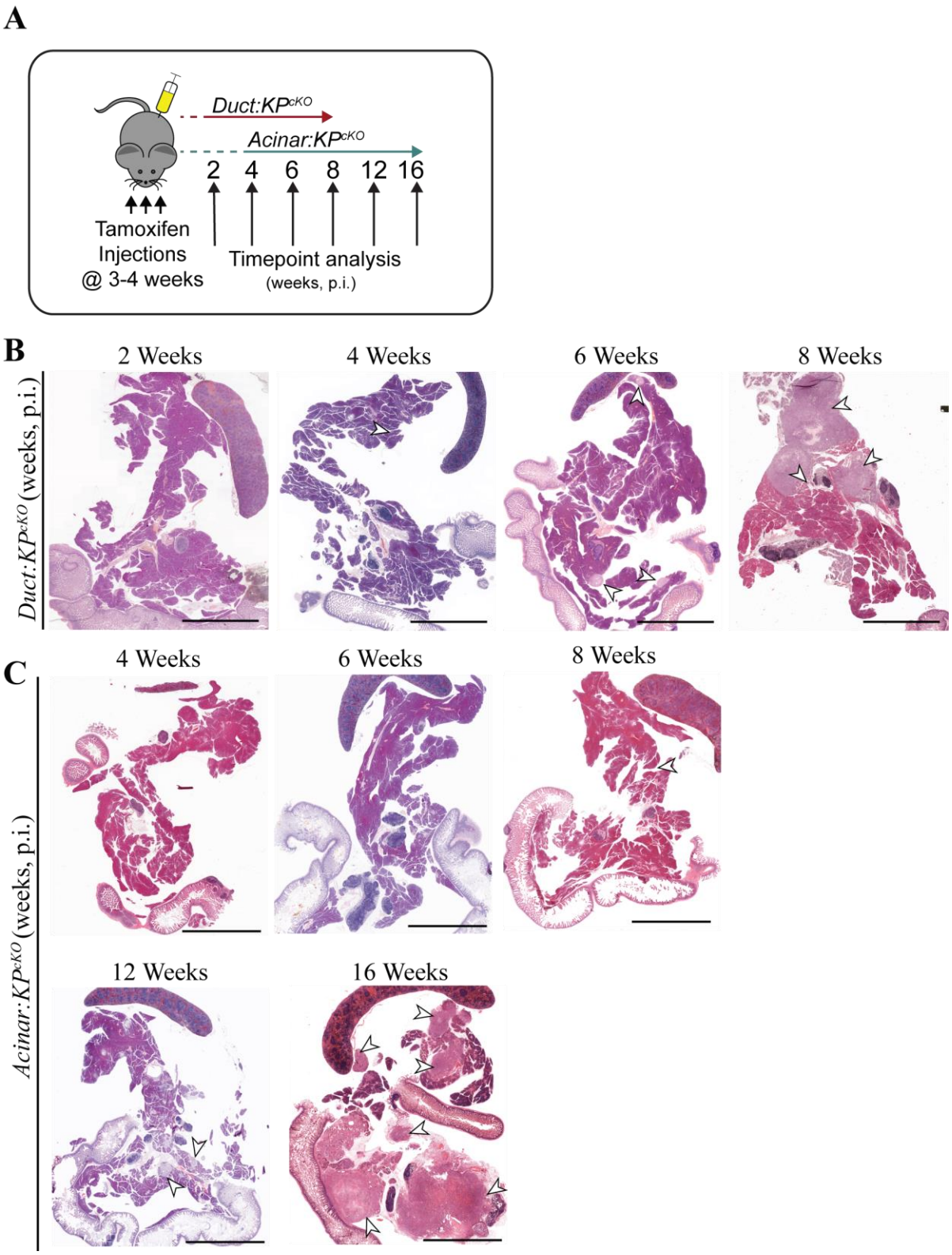

Figure 3.12 Quantification of tumor development in *Duct:KP^{cKO}* and *Acinar:KP^{cKO}* mice.

Figure 3.12 A) Schematic describing the experimental design. *Duct:KP^{cKO}* and *Acinar:KP^{cKO}* mice (n=3 for 2 wk p.i. *Duct:KP^{cKO}* mice and n= 4 for others) were injected with tamoxifen at 3-4 weeks of age and euthanized at 2, 4, 6 and 8 weeks post injection (p.i.) or 4, 6, 8, 12, and 16 weeks p.i. for *Duct:KP^{cKO}* or *Acinar:KP^{cKO}* mice, respectively. Representative whole section images of H&E stained tumors from **B**) *Duct:KP^{cKO}* and **C**) *Acinar:KP^{cKO}* mice at different time points post tamoxifen injection. Arrowheads indicate the location of tumors. **B**) *Duct:KP^{cKO}* mice developed small focal tumors as early as four weeks post injection. The number and size of the tumors further increased at six and eight weeks post injection. **C**) *Acinar:KP^{cKO}* mice developed small focal tumors after six weeks post injection. The number and size varied increased between 12 and 16 weeks post-injection. Ductal metaplasia comprised of small ductules and PanINs maintaining a lobular organization progressively increased from four to sixteen weeks post injection and displaced normal acinar cells in the pancreata from *Acinar:KP^{cKO}* mice. Scale: 5 mm (B-C).

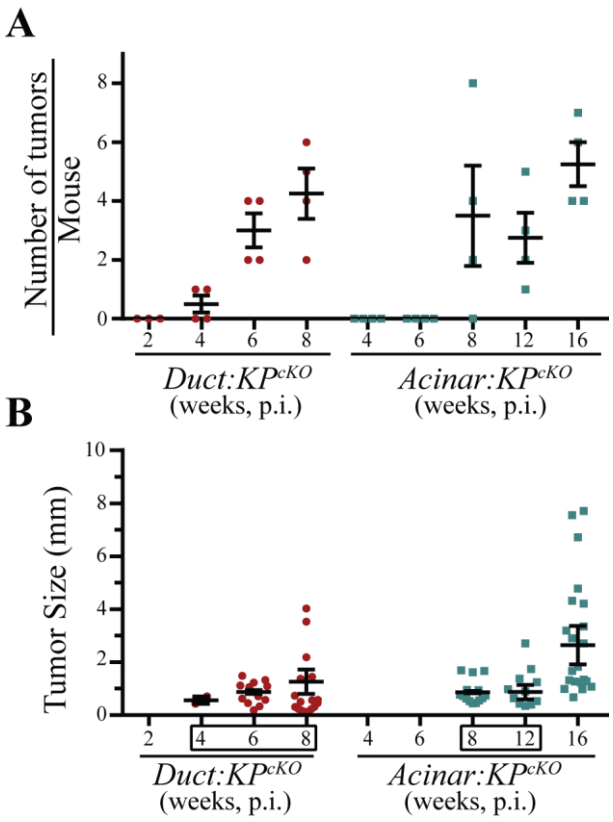

Figure 3.13 Tumors are present earlier and accumulate more rapidly in *Duct:KP^{cKO}* compared to *Acinar:KP^{cKO}* mice.

Figure 3.13 A) Quantification of the number of tumors present in *Duct:KP^{cKO}* and *Acinar:KP^{cKO}* mice revealed that *Duct:KP^{cKO}* mice developed tumors two weeks earlier than *Acinar:KP^{cKO}* mice. In addition, the number of tumors present increased consistently earlier in *Duct:KP^{cKO}* mice compared to *Acinar:KP^{cKO}* mice. **B**) Quantification of cross-sectional diameter of individual tumors (tumor size) in *Duct:KP^{cKO}* and *Acinar:KP^{cKO}* mice at different time points suggests that ductal-cell-derived tumors expanded rapidly between the four week span between four to eight weeks post tamoxifen injection (boxed). The size of acinar cell derived tumors were similar at 12 weeks post injection with the *Duct:KP^{cKO}* six week time point.

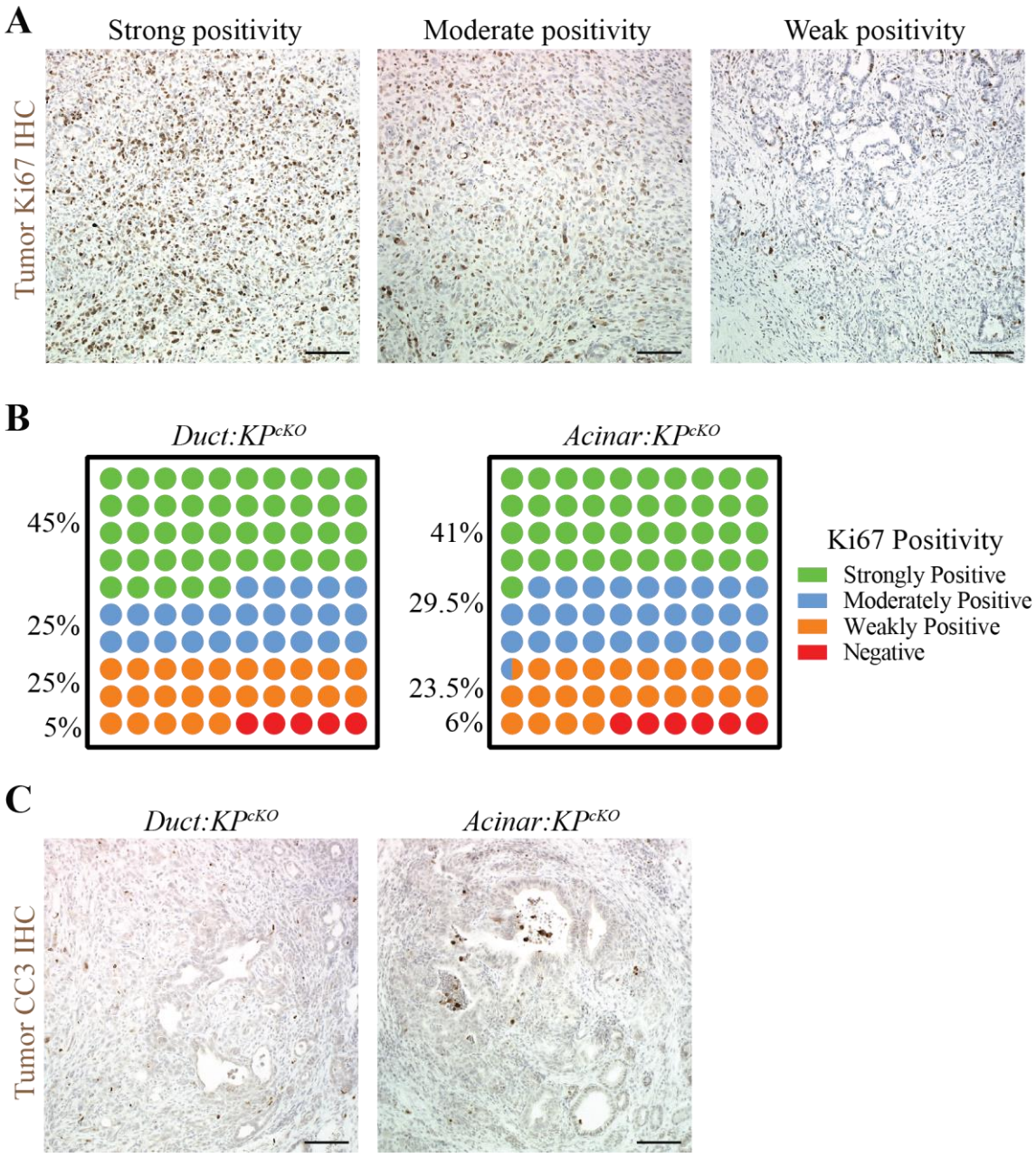

Figure 3.14 Tumors in *Duct:KP^{cKO}* and *Acinar:KP^{cKO}* mouse models do not significantly differ in cellular proliferation (Ki67) or apoptosis (CC3).

Figure 3.14 Both *Duct:KP^{cKO}*and *Acinar:KP^{cKO}* mouse models were analyzed for differences in growth by staining for Ki67 (proliferation marker) and cleaved caspase 3 (CC3, apoptosis marker). **A**) Representative images of Ki67 classification into groups of varying positivity levels. High positivity (>70% positive), moderate positivity (30-70%), weak positivity (1-30%) and no positivity (0%. not shown) were assigned to each tumor belonging to mice of varying ages. **B**) Quantitative analyses of tumors from *Duct:KP^{cKO}* and *Acinar:KP^{cKO}* models revealed that Ki67 expression in duct and acinar cell derived tumors were similar. **C**) Tumors analyzed from both *Duct:KP^{cKO}* and *Acinar:KP^{cKO}* mouse models had uniformly low, to no positivity for CC3 expression. Scale bar: 100 µm.

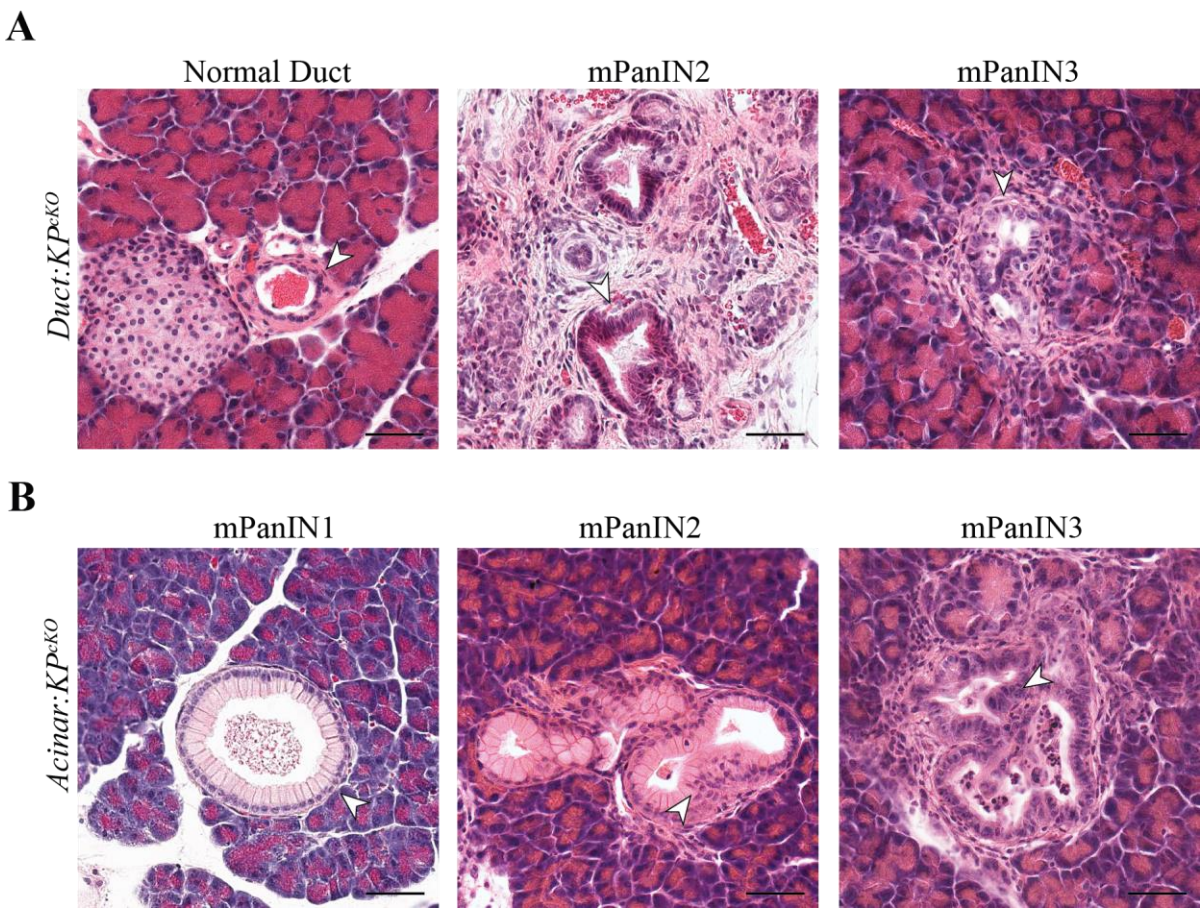

Figure 3.15 Concomitant Kras^{G12D} expression and *Trp53* loss induces a spectrum of mPanIN lesions from acinar cells but only high-grade mPanIN lesions from ductal cells.

A) Representative H&E images of a normal duct (arrowhead), mPanIN2 and mPanIN3 lesions (arrowhead) found in *Duct:KP^{cKO}* mice; no mPanIN1 lesions were found in the tissues analyzed. **B**) Representative H&E images of mPanIN1, mPanIN2, and mPanIN3 lesions observed in *Acinar:KP^{cKO}* mice. Scale bar: 50 μm (A-B).

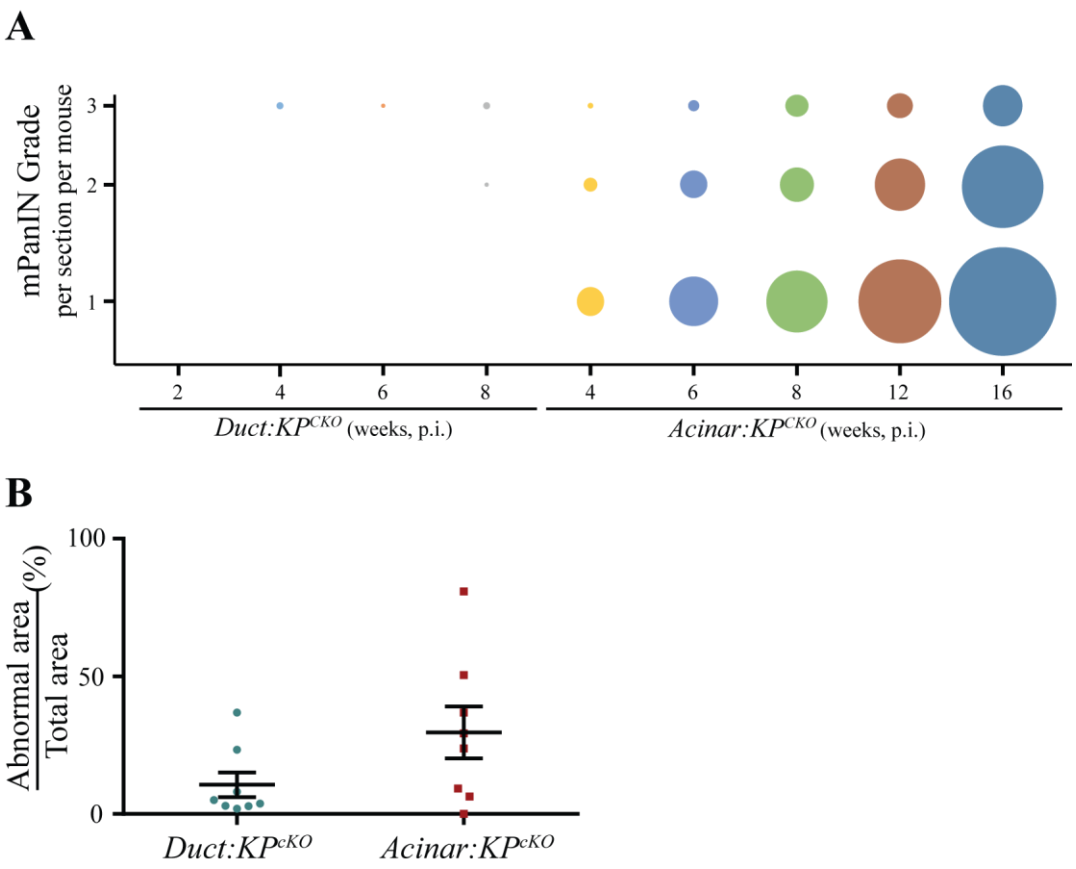

Figure 3.16 *Acinar:KP^{cKO}* mice display evidence for mPanIN accumulation and progression while *Duct:KP^{cKO}* mice only form high-grade precursor lesions (PanIN3).

A) Quantification of the number of mPanIN lesions of each grade at different time points in *Duct:KP^{cKO}* and *Acinar:KP^{cKO}* mice. Since the number of mPanIN1 in the *Acinar:KP^{cKO}* line at 16 weeks post injection had the highest number of lesions in our analysis, its relative size in the figure was used as the standard size and all remaining circles represent the fraction of mPanIN present relative to the standard. **B**) *Acinar:KP^{cKO}* mice can develop more metaplastic ducts and lesions than *Duct:KP^{cKO}* mice, as shown by its higher ratio of abnormal (non-tumor) to total pancreatic area at humane endpoint.

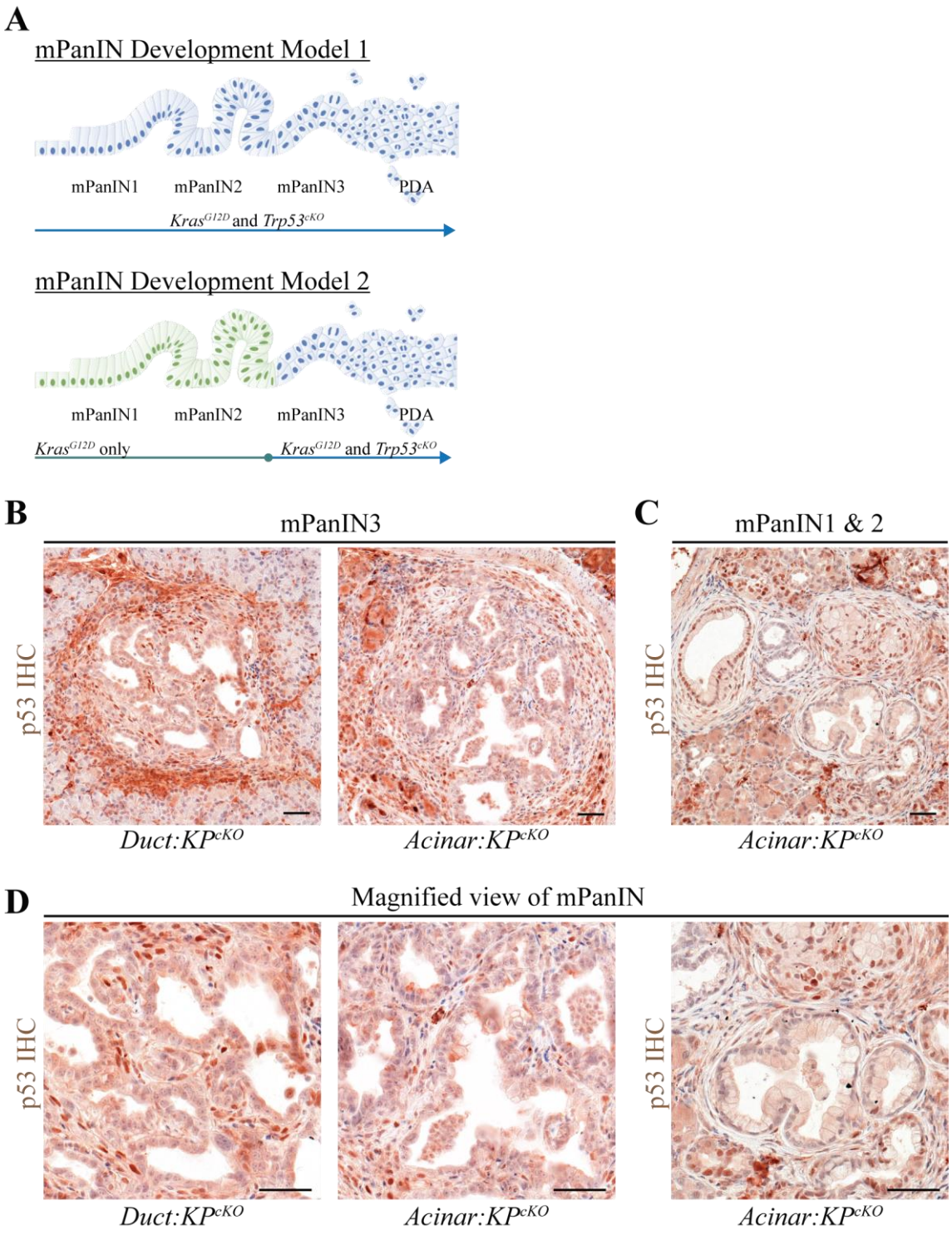

Figure 3.17 Representative images of p53 expression in precursor lesions from *Duct:KP^{cKO}* and *Acinar:KP^{cKO}* mouse models.

Figure 3.17 To confirm that the presence of low-grade mPanIN lesions in the *Acinar:KP^{cKO}* mouse model was not due to inefficient recombination, p53 expression in mPanIN of various grades from both the ductal and acinar cell specific models was analyzed. **A**) Schematic detailing two possible models to explain observed differences in mPanIN initiation and progression between *Duct:KP^{cKO}* and *Acinar:KP^{cKO}* mice. **B**) Near uniform loss of p53 expression was observed in high-grade lesions (mPanIN3, carcinoma-in-situ) from mouse models of both cell types. **C**) Low-grade *Acinar:KP^{cKO}* lesions (mPanIN1 and mPanIN2) showed variable p53 expression; some still expressed the tumor suppressor protein, p53, while others did not. Immune and stromal cell infiltrates were often positive for p53 and served as an internal positive control. **D**) Magnified view of mPanIN3 from *Acinar:KP^{cKO}* and *Duct:KP^{cKO}* mice and mPanIN1/2 from *Acinar:KP^{cKO}* mice, previously shown in A-C. Scale bars: 50 μm in A-C.

Table 3.1 Observed phenotypes from the survival cohort of *Duct:KP^{cKO}* and *Acinar:KP^{cKO}* mice at humane endpoint.

					Distant Met		Local invasion						
	Mouse ID	Age (days, p.i.)	Jaundice	Liver Lesion	Diaphragm	Peritoneum	Spleen	Duodenum	PNI/LVI/BVI	Ascites	CK19+	Cystic	Tumor Area (% of total pancreata)
Duct:KP^{cKO}	144	71			X	X	X	X	X		+++	0/7	90
	107	72	X	X				X			+++	0/4	41
	469	75	X	X				X		B	+++	0/10	48
	499	78		X					X	B	+++	0/4	92
	433	82		X				X			+++	0/8	87
	479	84		X	X	X			X	B	+++	0/5	86
	477	87									+++	0/5	42
	369	90						X			+++	0/5	42
Acinar:KP^{cKO}	97	105	X								+++	3/5	18
	23	121						X			+++	0/5	49
	94	124								C	+++	3/8	41
	27	125							X		+++	1/3	98
	100	128	X								+++	3/5	69
	52	140	X					X	X		+++	1/5	41
	92	146					X		X	B	+++	0/4	82
	33	160					X	X	X	C	+++	0/6	82

B = hemorrhagic (bloody) ascites fluid, C = clear ascites fluid, +++ = strong positive staining

Chapter 4. Discussion

I have shown that both ductal and acinar cells can give rise to PDAC when they are expressing oncogenic $Kras^{G12D}$ in the absence of *Trp53*. Unlike prior studies, I specifically examined cell of origin derived effects by inducing identical mutations in a cell-type specific manner. Although previous non-cell type specific and few cell type specific studies have shown that oncogenic Kras and p53 loss or mutation can rapidly induce PDAC (Bailey et al., 2016a; Bardeesy et al., 2006; Guerra et al., 2011; Hingorani et al., 2005), little is known about the impact of distinct cells of origin on tumor initiation, development and other tumor characteristics. In this study, I found that pancreatic ductal and acinar cells developed PDAC differently despite harboring identical initiating mutations. This suggests that cell of origin alone can significantly impact PDAC development, and provides insight into alternative pathways for tumor development.

4.1 Cell of origin and genotype affects PDAC initiation and development

I have demonstrated that both ductal and acinar cells expressing $Kras^{G12D}$ in the absence of p53 expression can give rise to PDAC, however, they do so with different developmental patterns. $Kras^{G12D}$-expressing ductal cells that have lost p53 expression initiated ductal carcinoma-in-situ (mPanIN3) rapidly and PDAC more efficiently without accompanying low-grade mPanIN formation; thus, resulting in a shortened survival time for this mouse model. In contrast, acinar cells with protumorigenic mutations ($Kras^{G12D}$ expression with *Trp53* deletion), a combination thought to be present only in high-grade lesions and PDAC (DiGiuseppe et al., 1994; Yamano et al., 2000), could still form low-grade mPanIN lesions similar to those found in $Kras^{G12D}$-only models (in addition to few *carcinoma in situ*, mPanIN3). These observations suggest a fundamental difference in the

developmental events occurring prior to PDAC forming from acinar versus ductal cells. On the one hand, acinar cells appear to require a transition through low-grade mPanIN to high-grade mPanIN before initiating PDAC. It suggests that mPanINs may be a part of an obligatory transition process between acinar cells and a transformed ductal-like cellular identity, regardless of the mutations present. The extended mPanIN transition negotiated by acinar cells, in turn, delays tumor initiation and subsequently prolongs survival in the *Acinar:KP^{cKO}* mice compared to the *Duct:KP^{cKO}* mice. On the other hand, ductal cells appeared to form low-grade mPanIN, albeit rarely, in the presence of oncogenic Kras only (Kopp et al., 2012; Ray et al., 2011). However, ductal cells may directly form carcinomas (mPanIN3 or PDAC) when stimulated by specific protumorigenic mutations– such as Kras^{G12D} in the absence of *Trp53*. This suggests that ductal cells could initiate PDAC by transition through a low-grade mPanIN state (like those observed by Kopp et al. (2012) and Ray et al. (2011)), if the *Kras* and *Trp53* mutations had occurred sequentially.

An argument could be made that the coarse nature of my time point analysis (2, 4, 6, and 8 week in *Duct:KP^{cKO}* and 4, 6, 8, 12, and 16 week in the *Acinar:KP^{cKO}* model) precluded the observation of low-grade ductal cell derived precursor lesions earlier on. However, even as tumor numbers continued to accumulate rapidly between 6 and 8 weeks post tamoxifen injection, no low-grade mPanIN1 were ever observed, and mPanIN3s also failed to accumulate over these time points. Analysis at a timepoint preceding the earliest observed tumor (ie. 4 weeks p.i.) found the pancreata of *Duct:KP^{cKO}* mice to be phenotypically normal at 2 weeks p.i., showing no tumors or lesions. This reinforced the notion that unlike ductal cells that only expressed Kras^{G12D} (Kopp et al., 2012), ductal cells expressing Kras^{G12D} that simultaneously lose *Trp53* do not form any low-grade mPanIN

lesions but proceed to directly initiate carcinomas (mPanIN3 or PDAC). Similar observations were made in a previous study using a *Hnf1b*^{CreER}*; Kras*$^{LSL\text{-}G12D}$*; Trp53*$^{LSL\text{-}R172H/LSL\text{-}R172H}$ mouse model, a model that targets ductal cells. In this study, the *Hnf1b*^{CreER} driven model did not form any mPanIN lesions – contrary to the rare *carcinoma in situ* that I report here. However, the lack of distinguishable mPanIN in their study could be explained by differing methodologies, their use of mutant gain-of-function *Trp53*^{R172H} rather than *Trp53*^{flox}, different drivers/mouse backgrounds, or other side effects due to the whole body loss of functional p53 (Bailey et al., 2016a). In the future, precursor specific lineage tracing studies may elucidate the different roles of ductal versus acinar cell derived mPanINs in PDAC initiation and development. For now, evidence suggests that ductal cells can give rise to mPanIN lesions, but unlike acinar cells, they may not always need to do so.

The reports I have mentioned thus far seem to firmly suggest that low-grade mPanIN lesions are more relevant for acinar cells than for ductal cells. Current evidence suggests that unlike acinar cells, low-grade mPanIN formation is not compulsory for ductal cells and in fact, any low-grade mPanIN that have emerged from ductal cells have not been directly linked to PDAC formation – casting further doubt on the relevance of low-grade ductal cell derived mPanIN and their initiation of PDAC (Bailey et al., 2016a; Kopp et al., 2012; Ray et al., 2011). However, unpublished data from our lab showed the direct emergence of PDAC from areas which morphologically resemble mPanIN1 or mPanIN2 lesions in a *Sox9CreER; Pten*$^{flox/flox}$ mouse model. This suggests that ductal cells can and do form mPanIN lesions of varying grades (mPanIN1-3) that directly contribute to tumorigenesis after a significant latency (>6 months), but only do so under appropriate genetic and microenvironmental conditions. These specific conditions appear to be different from those needed by acinar cells,

and have not been examined to date. Future studies interrogating the role of cell of origin in PDAC may begin to elucidate mechanistic differences behind ductal cell versus acinar cell initiated PDAC, and whether mPanIN from both cell types are functionally and transcriptionally equivalent despite the different genetic contexts in which they have been observed.

4.2 Pan-pancreatic mouse models of PDAC may initiate tumors from multiple cells of origin

Much work has been done to characterize the specific effects of genetic mutations on PDAC initiation and development, with most studies using pan-pancreatic mouse models such as *Pdx1-Cre* and *Ptf1a-Cre* recombinase drivers in combination with oncogenic Kras and loss/mutation of p53. However, evidence provided in a study by Bailey et al. (2016a) and evidence from this study would suggest that ductal and acinar cells actually respond differently depending on the type of *Trp53* mutation made and whether one or both alleles of *Trp53* were lost (Bailey et al., 2016a). Bailey et al. (2016a) found that acinar cells targeted by $Mist1^{CreER}; Kras^{LSL\text{-}G12D}; Trp53^{LSL\text{-}R172H/+}$ rapidly developed PDAC and succumbed to the disease less than 12 weeks after tamoxifen induced recombination. Similar mutations with ductal cells ($Hnf1bCreER; Kras^{LSL\text{-}G12D}; Trp53^{LSL\text{-}R172H/+}$) showed no phenotype up to three months post tamoxifen induced recombination. This was in stark contrast to the response of acinar cells to these mutations and further study demonstrated that ductal cells required homozygous *Trp53* mutations ($Hnf1bCreER; Kras^{LSL\text{-}G12D}; Trp53^{LSL\text{-}R172H/LSL\text{-}R172H}$) to similarly match the survival and phenotype of the acinar cell specific model. In contrast, evidence presented in this study has shown that simultaneous homozygous *Trp53* deletion in acinar or ductal cells expressing oncogenic $Kras^{G12D}$ leads to tumor development. In light of

these recent observations, there may be cell of origin specific effects at play in pan-pancreatic mouse models that have been previously unrecognized. For instance, whereas the first tumors observed in *Pdx1-Cre; Kras$^{LSL\text{-}G12D/+}$; Trp53$^{flox/+}$* or *Ptf1a$^{Cre/+}$; Kras$^{LSL\text{-}G12D}$; Trp53$^{R172H/+}$* could be acinar cell derived, initial tumors found in *Pdx1-Cre; Kras$^{LSL\text{-}G12D/+}$; Trp53$^{flox/flox}$* and *Ptf1a$^{Cre/+}$; Kras$^{LSL\text{-}G12D}$; Trp53$^{R172H/R172H}$* mice could instead be ductal cell derived due to faster carcinoma initiation from this cell type, as I have demonstrated in this thesis. However, other confounding factors such as any effect of the embryonic context, may complicate whether observations in cell type specific models could be simply extrapolated to the embryonic induced pancreatic cancer models. Because pancreatic tumors are likely initiated within a mature adult pancreatic environment, my studies emphasize the need to conduct studies in the adult context with specific cell types.

4.3 Cell of origin alters response to oncogenic stimiuli

I have shown that ductal and acinar cells respond differently when Kras^{G12D} is expressed and *Trp53* is deleted. Ductal cell specific mouse models developed no PDAC up to 16 months of age when only Kras^{G12D} expression is induced (Kopp et al., 2012), but rapidly developed PDAC in the absence of *Trp53*. In contrast, one study reported that acinar cells expressing Kras^{G12D} gave rise to PDAC by 12 months of age (Guerra et al., 2007), and by 4.5 months of age, when *Trp53* is lost. Collectively, these findings suggest that ductal cells and acinar cells can respond differently when subject to similar oncogenic stimuli.

Despite only developing few mPanIN when Kras^{G12D} is induced (Kopp et al., 2012; Ray et al., 2011), studies using pancreatic ductal epithelial cell (PDEC) cultures found that Kras^{G12D} expression resulted in increased cellular proliferation and suppressed p16-mediated senescence (Agbunag and Bar-Sagi, 2004; Diersch et al., 2016; Lee and Bar-Sagi, 2010).

These findings suggested that oncogenic Ras expression may prime the cell for tumor initiation. In agreement with this, Bailey et al. (2016a) observed no pancreatic changes in *Hnf1bCreER; Kras$^{LSL\text{-}G12D}$; Trp53$^{flox/+}$* mice up to three months post tamoxifen exposure. However, loss of both copies of *Trp53*, as in the *Duct:KP^{cKO}* mouse model, resulted in rapid tumor initiation. This suggests that p53 in ductal cells may be haplosufficient and retain enough function to suppress Kras^{G12D} mediated pro-proliferative signaling. Taken together, it appears that although ductal cells rarely form mPanIN upon oncogenic Ras expression, changes may be occurring which permit rapid proliferation and tumor initiation once conditions become favorable, such as a total loss of *Trp53*.

Acinar cells make up over 85% of the pancreas, forming the dominant cell population. Assuming *Kras$^{LSL\text{-}G12D}$* recombination levels are similar to those of *R26R$^{LSL\text{-}YFP}$*, my quantification would suggest that approximately 60% of all acinar cells were recombined and therefore express oncogenic Ras. Thus, it is expected that a significant number of acinar cells express Kras^{G12D} and form mPanIN. In spite of this, I only observed less than 300 mPanINs at 16 weeks post tamoxifen injection in the *Acinar:KP^{cKO}* mouse model. Potential explanations for this may be due to: a lower sensitivity to Kras oncogene expression, a requirement for embryonic program upregulation, and a presence of intrinsic arrest mechanisms in acinar cells. First, research has shown that oncogenic Kras expression in acinar cells requires inflammatory signaling to hyperactivate Kras to drive mPanIN formation (Daniluk et al., 2012). Therefore, establishment of the necessary feed-forward signaling to hyperactivate Ras may delay mPanIN initiation. Second, acinar-to-ductal reprogramming may add latency to mPanIN formation due to a requirement to promote embryonic ductal/progenitor programming. This is evidenced by studies showing that

expression of factors associated with embryonic programming drives mPanIN formation, and loss of such factors prevented mPanIN formation (De La O et al., 2008; Kopp et al., 2012). Finally, acinar cells could also have numerous cell intrinsic arrest mechanisms to prevent preneoplastic transition. For instance, acinar cells and acinar cell derived mPanINs have been shown to undergo senescence when the Ras kinase cascade is overactivated, either by culturing under Ras-stimulating conditions, or by oncogenic Kras expression in a mouse model, respectively (Guerra et al., 2011; Pinho et al., 2011a). In sum, acinar cells appear to require numerous conditions be met to initiate precursor lesions, delaying the acinar cell derived tumorigenic process.

An argument could be made that the observed precursor development differences in *Acinar:KP^{cKO}* mice may be due to inefficient recombination of the *Trp53$^{flox/flox}$* allele. However, two key reasons suggest this is not the case. First, because I am using identical alleles in both cell type specific mouse models, any inefficiencies due to large floxed alleles or position effects are likely to be reflected equally on both, since there are no changes in recombination size or position (Vooijs et al., 2001). Second and most importantly, the frequent observation of p53 negative, low-grade mPanIN1 lesions, (Figure 3.17B) suggests that even if acinar cell recombination was completely efficient, the developmental differences and delay observed between my models would continue to be observed. That is, the precursor progression seems to completely differ between the two cell type specific mouse models (*Duct:KP^{cKO}* and *Acinar:KP^{cKO}* mice). Importantly, this delay appears to extend to PanIN3 progression to PDAC from acinar cells, as these lesions are present very early on and p53 negative, but do not appear to efficiently generate PDAC. However, there remains the possibility that chromatin state differences between ductal and acinar cells may

make the *Trp53* locus more accessible in one cell type than the other. Thus, non-p53 expressing mPanIN1s in *Acinar:KP^{cKO}* mice may represent *Kras^{G12D}; Trp53$^{flox/+}$* or *Kras^{G12D}; Trp53$^{+/+}$* genotypes which have yet to upregulate *Trp53* expression (Figure 3.17A). To address this possibility, future laser capture microdissection or in-situ hybridization experiments would be needed to validate and quantify the *Trp53* locus recombination rate in low grade precursor lesions in the *Acinar:KP^{cKO}* mouse model.

4.4 Tumor heterogeneity arising from acinar cell dedifferentiation

In this study, I characterized tumors derived from ductal and acinar cells and found them to be similar in their differentiation status and type – moderate to poorly differentiated adenocarcinomas. However, acinar cell derived tumors displayed extra phenotypes not seen in tumors from the ductal cell specific model, and I have designated these additional phenotypes as precursor-like or cystic (Figure 3.7A-B). This suggests that acinar cells may be a source of additional tumor heterogeneity when compared to ductal cells.

One potential mechanism for acinar cells to generate additional heterogeneity could be via a stochastic acinar-to-ductal reprogramming process. Acinar cells are differentiated from a pancreatic progenitor cell after expression of acinar cell specifying factors such as Ptf1a, Rbp-jl and Nr5a2 (reviewed in Shih et al., 2013). Loss of these acinar cell specifying factors has been shown to accelerate and drive Kras^{G12D}-mediated mPanIN formation (Figura et al., 2014b; Krah et al., 2015). Concurrently, mPanIN formation is associated with expression of embryonic progenitor/ductal markers such as Pdx1, Hes1, Sox9, Hnf1b (Collins et al., 2012; Kopp et al., 2012). Furthermore, embryonic forms of protein complexes also become expressed instead of their adult versions, suggestive of an adoption of the embryonic transcriptional programme (Pinho et al., 2011a). These types of large scale

transcriptional network changes are closely regulated by epigenetic modifications (Yamada et al., 2014). Thus, loss of a chromatin remodeler, such as Brg1, may interfere with the necessary epigenetic modifications that need to be made. In support of this, *Brg1* deletion has been shown to result in severely diminished mPanIN formation in an acinar cell specific mouse model (Figura et al., 2014a).Taken together, these findings suggest that acinar cell derived PDAC undergoes dedifferentiation, after which transformation into PDAC may involve a more stochastic and random process; a process which could explain the heterogeneity seen in the *Acinar:KP^{cKO}* model, but not *Duct:KP^{cKO}* model. Specifically, I observed that the survival time for *Acinar:KP^{cKO}* mice ranged from 105 to 160 days, and the size of tumors varied widely at 12 weeks post injection. Furthermore, these mice also accumulated a large number of mPanIN over time, as well as developed additional tumor phenotypes that were seldom observed in *Duct:KP^{cKO}* mice (Figure 3.2B, Figure 3.7A-B, Figure 3.13A and B, and Figure 3.16A). These findings all suggest acinar cell transformation is more unpredictable, potentially due to the stochastic acinar-to-ductal-to-mPanIN-to-PDAC reprogramming process. Future studies examining the epigenetic and transcriptional processes of acinar-to-ductal reprogramming and mPanIN progression may yet identify mechanistic similarities with iPSC induction, a process which also appears stochastic and is currently not well understood (Takahashi and Yamanaka, 2016).

4.5 Catastrophic PDAC initiation from ductal cells

Current understanding of PDAC development suggests that mutations are accumulated in a stepwise manner: low-grade lesions acquire Kras and p16 alterations, while high-grade lesions acquire *Trp53* and *Smad4* mutations (Hruban et al., 2000). In my study, I found that combining an early mutation (*Kras^{G12D}*) with a late mutation (*Trp53$^{flox/flox}$*) in

ductal cells was sufficient to rapidly induce rapid carcinoma without forming any low-grade mPanIN lesions. In contrast, acinar cells with early and late mutations still appeared to go through the full spectrum of mPanIN stages. These findings suggest that ductal cells, under certain contexts, follow a PDAC developmental process distinct from acinar cells; one in which $Kras^{G12D}$ rarely induces mPanIN1 (Brembeck et al., 2003; Kopp et al., 2012; Ray et al., 2011), but introduction of *Trp53* loss rapidly causes formation of carcinomas. This pattern of development resembles "catastrophic PDAC progression", which was first suggested in 2003 (Real, 2003). In brief, Real, F.X. hypothesized that a catastrophic event may cause sudden and rapid progression of cancer and even bypass specific PanIN precursor lesion stages (Real, 2003). In contrast, acinar cells show a developmental pattern consistent with current linear PanIN progression schemes, as p53 loss did not induce a complete loss of individual low-grade mPanIN stages. In agreement with our current understanding of PanIN progression, low-grade human PanIN lesions are associated with $Kras^{G12D}$ mutations but not p53 (Kanda et al., 2012, 2013). Taken together, these observations suggest that cell of origin, in combination with mutational composition; can impact the developmental trajectory of PDAC. Thus, the current PanIN progression model (cite your first diagram figure from intro) may only capture a simplified picture of the way tumors develop and this model may need to be revised to incorporate the context of specific genetic mutations and cells of origin (see Appendix A, Figure A.1).

4.6 Closing remarks and future directions

I have shown in this study that cell of origin is an important factor to consider when using mouse models to study PDAC. It can affect tumor progression, phenotype, and may one day even change how PDAC can be detected and treated. Before that can happen, further

characterization of the relevance of cell of origin in PDAC is needed. Future studies should first determine acinar cell specific and ductal cell specific tumor signatures, then identify whether they are present in human PDAC. Although my study has demonstrated that both acinar and ductal cells can give rise to cancer under identical genetic conditions, the method of inducing genetic changes in mice may make it difficult to apply these results directly to human disease. For instance, the induction of $Kras^{G12D}$ expression in large numbers of acinar cells or the simultaneous activation of multiple disease relevant gene mutations is generally thought to not occur in humans. One could hypothesize that acinar cells may typically undergo senescence and cell death in response to Kras mutations; therefore, the seemingly quiescent ductal cells may actually represent the prime source of PDAC. This is despite the lack of widespread phenotypic changes in ductal cells when *Kras* is altered. In sum, efforts should now be made to identify the relevance of cell of origin in PDAC, since this study and others (Bailey et al., 2016a; Figura et al., 2014a) have begun to demonstrate that acinar and ductal cells can differ significantly in their tumorigenic potential under certain contexts.

References

Agbunag, C., and Bar-Sagi, D. (2004). Oncogenic K-ras Drives Cell Cycle Progression and Phenotypic Conversion of Primary Pancreatic Duct Epithelial Cells. Cancer Res. *64*, 5659–5663.

Andea, A., Sarkar, F., and Adsay, V.N. (2003). Clinicopathological Correlates of Pancreatic Intraepithelial Neoplasia: A Comparative Analysis of 82 Cases With and 152 Cases Without Pancreatic Ductal Adenocarcinoma. Mod. Pathol. *16*, 996–1006.

Bailey, J.M., Hendley, A.M., Lafaro, K.J., Pruski, M.A., Jones, N.C., Alsina, J., Younes, M., Maitra, A., McAllister, F., Iacobuzio-Donahue, C.A., et al. (2016a). p53 mutations cooperate with oncogenic Kras to promote adenocarcinoma from pancreatic ductal cells. Oncogene *35*, 4282–4288.

Bailey, P., Chang, D.K., Nones, K., Johns, A.L., Patch, A.-M., Gingras, M.-C., Miller, D.K., Christ, A.N., Bruxner, T.J.C., Quinn, M.C., et al. (2016b). Genomic analyses identify molecular subtypes of pancreatic cancer. Nature *531*, 47–52.

Bardeesy, N., Aguirre, A.J., Chu, G.C., Cheng, K.-H., Lopez, L.V., Hezel, A.F., Feng, B., Brennan, C., Weissleder, R., Mahmood, U., et al. (2006). Both p16(Ink4a) and the p19(Arf)-p53 pathway constrain progression of pancreatic adenocarcinoma in the mouse. Proc. Natl. Acad. Sci. U. S. A. *103*, 5947–5952.

Blanpain, C. (2013). Tracing the cellular origin of cancer. Nat. Cell Biol. *15*, 126–134.

Brat, D.J., Lillemoe, K.D., Yeo, C.J., Warfield, P.B., and Hruban, R.H. (1998). Progression of pancreatic intraductal neoplasias to infiltrating adenocarcinoma of the pancreas. Am. J. Surg. Pathol. *22*, 163–169.

Brembeck, F.H., Schreiber, F.S., Deramaudt, T.B., Craig, L., Rhoades, B., Swain, G., Grippo, P., Stoffers, D.A., Silberg, D.G., and Rustgi, A.K. (2003). The Mutant K-ras Oncogene Causes Pancreatic Periductal Lymphocytic Infiltration and Gastric Mucous Neck Cell Hyperplasia in Transgenic Mice. Cancer Res. *63*, 2005–2009.

Brockie, E., Anand, A., and Albores-Saavedra, J. (1998). Progression of atypical ductal hyperplasia/carcinoma in situ of the pancreas to invasive adenocarcinoma. Ann. Diagn. Pathol. *2*, 286–292.

Choi, N., Zhang, B., Zhang, L., Ittmann, M., and Xin, L. (2012). Adult murine prostate basal and luminal cells are self-sustained lineages that can both serve as targets for prostate cancer initiation. Cancer Cell *21*, 253–265.

Collins, M.A., Bednar, F., Zhang, Y., Brisset, J.-C., Galbán, S., Galbán, C.J., Rakshit, S., Flannagan, K.S., Adsay, N.V., and Pasca di Magliano, M. (2012). Oncogenic Kras is required for both the initiation and maintenance of pancreatic cancer in mice. J. Clin. Invest. *122*, 639–653.

Collisson, E.A., Sadanandam, A., Olson, P., Gibb, W.J., Truitt, M., Gu, S., Cooc, J., Weinkle, J., Kim, G.E., Jakkula, L., et al. (2011). Subtypes of Pancreatic Ductal Adenocarcinoma and Their Differing Responses to Therapy. Nat. Med. *17*, 500–503.

Coppoolse, E.R., Vroomen, M.J. de, Gennip, F. van, Hersmus, B.J.M., and Haaren, M.J.J. van (2005). Size Does Matter: Cre-mediated Somatic Deletion Efficiency Depends on the Distance Between the Target lox. Plant Mol. Biol. *58*, 687–698.

Cubilla, A.L., and Fitzgerald, P.J. (1976). Morphological lesions associated with human primary invasive nonendocrine pancreas cancer. Cancer Res. *36*, 2690–2698.

Daniluk, J., Liu, Y., Deng, D., Chu, J., Huang, H., Gaiser, S., Cruz-Monserrate, Z., Wang, H., Ji, B., and Logsdon, C.D. (2012). An NF-κB pathway–mediated positive feedback loop amplifies Ras activity to pathological levels in mice. J. Clin. Invest. *122*, 1519–1528.

De La O, J.-P., Emerson, L.L., Goodman, J.L., Froebe, S.C., Illum, B.E., Curtis, A.B., and Murtaugh, L.C. (2008). Notch and Kras reprogram pancreatic acinar cells to ductal intraepithelial neoplasia. Proc. Natl. Acad. Sci. U. S. A. *105*, 18907–18912.

Diersch, S., Wirth, M., Schneeweis, C., Jörs, S., Geisler, F., Siveke, J.T., Rad, R., Schmid, R.M., Saur, D., Rustgi, A.K., et al. (2016). KrasG12D induces EGFR-MYC cross signaling in murine primary pancreatic ductal epithelial cells. Oncogene *35*, 3880–3886.

DiGiuseppe, J.A., Hruban, R.H., Goodman, S.N., Polak, M., van den Berg, F.M., Allison, D.C., Cameron, J.L., and Offerhaus, G.J. (1994). Overexpression of p53 protein in adenocarcinoma of the pancreas. Am. J. Clin. Pathol. *101*, 684–688.

Figura, G. von, Fukuda, A., Roy, N., Liku, M.E., Morris Iv, J.P., Kim, G.E., Russ, H.A., Firpo, M.A., Mulvihill, S.J., Dawson, D.W., et al. (2014a). The chromatin regulator Brg1 suppresses formation of intraductal papillary mucinous neoplasm and pancreatic ductal adenocarcinoma. Nat. Cell Biol. *16*, 255–267.

Figura, G. von, Morris, J.P., Wright, C.V.E., and Hebrok, M. (2014b). Nr5a2 maintains acinar cell differentiation and constrains oncogenic Kras-mediated pancreatic neoplastic initiation. Gut *63*, 656–664.

Font-Burgada, J., Shalapour, S., Ramaswamy, S., Hsueh, B., Rossell, D., Umemura, A., Taniguchi, K., Nakagawa, H., Valasek, M.A., Ye, L., et al. (2015). Hybrid Periportal Hepatocytes Regenerate the Injured Liver without Giving Rise to Cancer. Cell *162*, 766–779.

Furukawa, T., Chiba, R., Kobari, M., Matsuno, S., Nagura, H., and Takahashi, T. (1994). Varying grades of epithelial atypia in the pancreatic ducts of humans. Classification based on morphometry and multivariate analysis and correlated with positive reactions of carcinoembryonic antigen. Arch. Pathol. Lab. Med. *118*, 227–234.

Guerra, C., Schuhmacher, A.J., Cañamero, M., Grippo, P.J., Verdaguer, L., Pérez-Gallego, L., Dubus, P., Sandgren, E.P., and Barbacid, M. (2007). Chronic pancreatitis is essential for

induction of pancreatic ductal adenocarcinoma by K-Ras oncogenes in adult mice. Cancer Cell *11*, 291–302.

Guerra, C., Collado, M., Navas, C., Schuhmacher, A.J., Hernández-Porras, I., Cañamero, M., Rodriguez-Justo, M., Serrano, M., and Barbacid, M. (2011). Pancreatitis-Induced Inflammation Contributes to Pancreatic Cancer by Inhibiting Oncogene-Induced Senescence. Cancer Cell *19*, 728–739.

Habbe, N., Shi, G., Meguid, R.A., Fendrich, V., Esni, F., Chen, H., Feldmann, G., Stoffers, D.A., Konieczny, S.F., Leach, S.D., et al. (2008). Spontaneous induction of murine pancreatic intraepithelial neoplasia (mPanIN) by acinar cell targeting of oncogenic Kras in adult mice. Proc. Natl. Acad. Sci. U. S. A. *105*, 18913–18918.

Hingorani, S.R., Petricoin, E.F., Maitra, A., Rajapakse, V., King, C., Jacobetz, M.A., Ross, S., Conrads, T.P., Veenstra, T.D., Hitt, B.A., et al. (2003). Preinvasive and invasive ductal pancreatic cancer and its early detection in the mouse. Cancer Cell *4*, 437–450.

Hingorani, S.R., Wang, L., Multani, A.S., Combs, C., Deramaudt, T.B., Hruban, R.H., Rustgi, A.K., Chang, S., and Tuveson, D.A. (2005). Trp53R172H and KrasG12D cooperate to promote chromosomal instability and widely metastatic pancreatic ductal adenocarcinoma in mice. Cancer Cell *7*, 469–483.

Howlader, N., Noone, A., Krapcho, M., Miller, D., Bishop, K., Altekruse, S., Kosary, C., Yu, M., Ruhl, J., Tatalovich, Z., et al. (2016). SEER Cancer Statistics Review, 1975-2013.

Hruban, R.H., van Mansfeld, A.D., Offerhaus, G.J., van Weering, D.H., Allison, D.C., Goodman, S.N., Kensler, T.W., Bose, K.K., Cameron, J.L., and Bos, J.L. (1993). K-ras oncogene activation in adenocarcinoma of the human pancreas. A study of 82 carcinomas using a combination of mutant-enriched polymerase chain reaction analysis and allele-specific oligonucleotide hybridization. Am. J. Pathol. *143*, 545–554.

Hruban, R.H., Goggins, M., Parsons, J., and Kern, S.E. (2000). Progression Model for Pancreatic Cancer. Clin. Cancer Res. *6*, 2969–2972.

Hruban, R.H., Maitra, A., and Goggins, M. (2008). Update on Pancreatic Intraepithelial Neoplasia. Int. J. Clin. Exp. Pathol. *1*, 306–316.

Inada, A., Nienaber, C., Katsuta, H., Fujitani, Y., Levine, J., Morita, R., Sharma, A., and Bonner-Weir, S. (2008). Carbonic anhydrase II-positive pancreatic cells are progenitors for both endocrine and exocrine pancreas after birth. Proc. Natl. Acad. Sci. U. S. A. *105*, 19915–19919.

Ji, B., Tsou, L., Wang, H., Gaiser, S., Chang, D.Z., Daniluk, J., Bi, Y., Grote, T., Longnecker, D.S., and Logsdon, C.D. (2009). Ras activity levels control the development of pancreatic diseases. Gastroenterology *137*, 1072–1082, 1082-6.

Kanda, M., Matthaei, H., Wu, J., Hong, S., Yu, J., Borges, M., Hruban, R.H., Maitra, A., Kinzler, K., Vogelstein, B., et al. (2012). Presence of Somatic Mutations in Most Early-Stage Pancreatic Intraepithelial Neoplasia. Gastroenterology *142*, 730–733.e9.

Kanda, M., Sadakari, Y., Borges, M., Topazian, M., Farrell, J., Syngal, S., Lee, J., Kamel, I., Lennon, A.M., Knight, S., et al. (2013). Mutant TP53 in Duodenal Samples of Pancreatic Juice From Patients With Pancreatic Cancer or High-Grade Dysplasia. Clin. Gastroenterol. Hepatol. *11*, 719–730.e5.

Kopinke, D., Brailsford, M., Pan, F.C., Magnuson, M.A., Wright, C.V.E., and Murtaugh, L.C. (2012). Ongoing Notch signaling maintains phenotypic fidelity in the adult exocrine pancreas. Dev. Biol. *362*, 57–64.

Kopp, J.L., Dubois, C.L., Schaffer, A.E., Hao, E., Shih, H.P., Seymour, P.A., Ma, J., and Sander, M. (2011). Sox9+ ductal cells are multipotent progenitors throughout development but do not produce new endocrine cells in the normal or injured adult pancreas. Development *138*, 653–665.

Kopp, J.L., von Figura, G., Mayes, E., Liu, F.-F., Dubois, C.L., Morris, J.P., Pan, F.C., Akiyama, H., Wright, C.V.E., Jensen, K., et al. (2012). Identification of Sox9-dependent acinar-to-ductal reprogramming as the principal mechanism for initiation of pancreatic ductal adenocarcinoma. Cancer Cell *22*, 737–750.

Kozuka, S., Sassa, R., Taki, T., Masamoto, K., Nagasawa, S., Saga, S., Hasegawa, K., and Takeuchi, M. (1979). Relation of pancreatic duct hyperplasia to carcinoma. Cancer *43*, 1418–1428.

Krah, N.M., De La O, J.-P., Swift, G.H., Hoang, C.Q., Willet, S.G., Chen Pan, F., Cash, G.M., Bronner, M.P., Wright, C.V., Macdonald, R.J., et al. (2015). The acinar differentiation determinant PTF1A inhibits initiation of pancreatic ductal adenocarcinoma. eLife *4*.

Lee, K.E., and Bar-Sagi, D. (2010). Oncogenic KRas suppresses inflammation-associated senescence of pancreatic ductal cells. Cancer Cell *18*, 448–458.

Lu, T.-L., Huang, Y.-F., You, L.-R., Chao, N.-C., Su, F.-Y., Chang, J.-L., and Chen, C.-M. (2013). Conditionally Ablated Pten in Prostate Basal Cells Promotes Basal-to-Luminal Differentiation and Causes Invasive Prostate Cancer in Mice. Am. J. Pathol. *182*, 975–991.

Marino, S., Vooijs, M., van der Gulden, H., Jonkers, J., and Berns, A. (2000). Induction of medulloblastomas in p53-null mutant mice by somatic inactivation of Rb in the external granular layer cells of the cerebellum. Genes Dev. *14*, 994–1004.

Means, A.L., Xu, Y., Zhao, A., Ray, K.C., and Gu, G. (2008). A CK19CreERT knockin mouse line allows for conditional DNA recombination in epithelial cells in multiple endodermal organs. Genesis *46*, 318–323.

Moffitt, R.A., Marayati, R., Flate, E.L., Volmar, K.E., Loeza, S.G.H., Hoadley, K.A., Rashid, N.U., Williams, L.A., Eaton, S.C., Chung, A.H., et al. (2015). Virtual microdissection

identifies distinct tumor- and stroma-specific subtypes of pancreatic ductal adenocarcinoma. Nat. Genet. *47*, 1168–1178.

Morris, J.P., Cano, D.A., Sekine, S., Wang, S.C., and Hebrok, M. (2010). β-catenin blocks Kras-dependent reprogramming of acini into pancreatic cancer precursor lesions in mice. J. Clin. Invest. *120*, 508–520.

Noll, E.M., Eisen, C., Stenzinger, A., Espinet, E., Muckenhuber, A., Klein, C., Vogel, V., Klaus, B., Nadler, W., Rösli, C., et al. (2016). CYP3A5 mediates basal and acquired therapy resistance in different subtypes of pancreatic ductal adenocarcinoma. Nat. Med. *22*, 278–287.

Pan, F.C., Bankaitis, E.D., Boyer, D., Xu, X., Van de Casteele, M., Magnuson, M.A., Heimberg, H., and Wright, C.V.E. (2013). Spatiotemporal patterns of multipotentiality in Ptf1a-expressing cells during pancreas organogenesis and injury-induced facultative restoration. Dev. Camb. Engl. *140*, 751–764.

Park, J.W., Lee, J.K., Phillips, J.W., Huang, P., Cheng, D., Huang, J., and Witte, O.N. (2016). Prostate epithelial cell of origin determines cancer differentiation state in an organoid transformation assay. Proc. Natl. Acad. Sci. *113*, 4482–4487.

Pinho, A.V., Rooman, I., Reichert, M., Medts, N.D., Bouwens, L., Rustgi, A.K., and Real, F.X. (2011a). Adult pancreatic acinar cells dedifferentiate to an embryonic progenitor phenotype with concomitant activation of a senescence programme that is present in chronic pancreatitis. Gut *60*, 958–966.

Pinho, A.V., Rooman, I., and Real, F.X. (2011b). p53-dependent regulation of growth, epithelial-mesenchymal transition and stemness in normal pancreatic epithelial cells. Cell Cycle *10*, 1312–1321.

Rahib, L., Smith, B.D., Aizenberg, R., Rosenzweig, A.B., Fleshman, J.M., and Matrisian, L.M. (2014). Projecting Cancer Incidence and Deaths to 2030: The Unexpected Burden of Thyroid, Liver, and Pancreas Cancers in the United States. Cancer Res. *74*, 2913–2921.

Ray, K.C., Bell, K.M., Yan, J., Gu, G., Chung, C.H., Washington, M.K., and Means, A.L. (2011). Epithelial Tissues Have Varying Degrees of Susceptibility to Kras G12D -Initiated Tumorigenesis in a Mouse Model. PLOS ONE *6*, e16786.

Real, F.X. (2003). A “catastrophic hypothesis” for pancreas cancer progression1. Gastroenterology *124*, 1958–1964.

Roy, N., Takeuchi, K.K., Ruggeri, J.M., Bailey, P., Chang, D., Li, J., Leonhardt, L., Puri, S., Hoffman, M.T., Gao, S., et al. (2016). PDX1 dynamically regulates pancreatic ductal adenocarcinoma initiation and maintenance. Genes Dev. *30*, 2669–2683.

Scarpa, A., Capelli, P., Mukai, K., Zamboni, G., Oda, T., Iacono, C., and Hirohashi, S. (1993). Pancreatic adenocarcinomas frequently show p53 gene mutations. Am. J. Pathol. *142*, 1534–1543.

Schnitt, S.J. (2010). Classification and prognosis of invasive breast cancer: from morphology to molecular taxonomy. Mod. Pathol. *23*, S60–S64.

Schwartz, A.M., and Henson, D.E. (2007). Familial and sporadic pancreatic carcinoma, epidemiologic concordance. Am. J. Surg. Pathol. *31*, 645–646.

Shi, G., Zhu, L., Sun, Y., Bettencourt, R., Damsz, B., Hruban, R.H., and Konieczny, S.F. (2009). Loss of the acinar-restricted transcription factor Mist1 accelerates Kras-induced pancreatic intraepithelial neoplasia. Gastroenterology *136*, 1368–1378.

Shih, H.P., Wang, A., and Sander, M. (2013). Pancreas Organogenesis: From Lineage Determination to Morphogenesis. Annu. Rev. Cell Dev. Biol. *29*, 81–105.

Solar, M., Cardalda, C., Houbracken, I., Martín, M., Maestro, M.A., De Medts, N., Xu, X., Grau, V., Heimberg, H., Bouwens, L., et al. (2009). Pancreatic Exocrine Duct Cells Give Rise to Insulin-Producing β Cells during Embryogenesis but Not after Birth. Dev. Cell *17*, 849–860.

Srinivas, S., Watanabe, T., Lin, C.-S., William, C.M., Tanabe, Y., Jessell, T.M., and Costantini, F. (2001). Cre reporter strains produced by targeted insertion of EYFP and ECFP into the ROSA26 locus. BMC Dev. Biol. *1*, 4.

Swidnicka-Siergiejko, A.K., Gomez-Chou, S.B., Cruz-Monserrate, Z., Deng, D., Liu, Y., Huang, H., Ji, B., Azizian, N., Daniluk, J., Lu, W., et al. (2016). Chronic inflammation initiates multiple forms of K-Ras-independent mouse pancreatic cancer in the absence of TP53. Oncogene.

Takahashi, K., and Yamanaka, S. (2016). A decade of transcription factor-mediated reprogramming to pluripotency. Nat. Rev. Mol. Cell Biol. *17*, 183–193.

Teague, A., Lim, K.-H., and Wang-Gillam, A. (2015). Advanced pancreatic adenocarcinoma: a review of current treatment strategies and developing therapies. Ther. Adv. Med. Oncol. *7*, 68–84.

Tuveson, D.A., Shaw, A.T., Willis, N.A., Silver, D.P., Jackson, E.L., Chang, S., Mercer, K.L., Grochow, R., Hock, H., Crowley, D., et al. (2004). Endogenous oncogenic K-ras(G12D) stimulates proliferation and widespread neoplastic and developmental defects. Cancer Cell *5*, 375–387.

Visvader, J.E. (2011). Cells of origin in cancer. Nature *469*, 314+.

Vooijs, M., Jonkers, J., and Berns, A. (2001). A highly efficient ligand-regulated Cre recombinase mouse line shows that LoxP recombination is position dependent. EMBO Rep. *2*, 292–297.

Wagner, M., Lührs, H., Klöppel, G., Adler, G., and Schmid, R.M. (1998). Malignant transformation of duct-like cells originating from acini in transforming growth factor α transgenic mice. Gastroenterology *115*, 1254–1262.

Wagner, M., Greten, F.R., Weber, C.K., Koschnick, S., Mattfeldt, T., Deppert, W., Kern, H., Adler, G., and Schmid, R.M. (2001). A murine tumor progression model for pancreatic cancer recapitulating the genetic alterations of the human disease. Genes Dev. *15*, 286–293.

Wang, Z.A., Mitrofanova, A., Bergren, S.K., Abate-Shen, C., Cardiff, R.D., Califano, A., and Shen, M.M. (2013). Lineage analysis of basal epithelial cells reveals their unexpected plasticity and supports a cell of origin model for prostate cancer heterogeneity. Nat. Cell Biol. *15*, 274–283.

Wilentz, R.E., Iacobuzio-Donahue, C.A., Argani, P., McCarthy, D.M., Parsons, J.L., Yeo, C.J., Kern, S.E., and Hruban, R.H. (2000). Loss of expression of Dpc4 in pancreatic intraepithelial neoplasia: evidence that DPC4 inactivation occurs late in neoplastic progression. Cancer Res. *60*, 2002–2006.

Yamada, Y., Haga, H., and Yamada, Y. (2014). Concise Review: Dedifferentiation Meets Cancer Development: Proof of Concept for Epigenetic Cancer. Stem Cells Transl. Med. *3*, 1182–1187.

Yamano, M., Fujii, H., Takagaki, T., Kadowaki, N., Watanabe, H., and Shirai, T. (2000). Genetic progression and divergence in pancreatic carcinoma. Am. J. Pathol. *156*, 2123–2133.

Yersal, O., and Barutca, S. (2014). Biological subtypes of breast cancer: Prognostic and therapeutic implications. World J. Clin. Oncol. *5*, 412–424.

Zheng, B., Sage, M., Sheppeard, E.A., Jurecic, V., and Bradley, A. (2000). Engineering Mouse Chromosomes with Cre-loxP: Range, Efficiency, and Somatic Applications. Mol. Cell. Biol. *20*, 648–655.

Appendices

Appendix A PanIN progression from ductal versus acinar cells.

A.1 PDAC development using *Kras*^{G12D} and *Trp53*$^{flox/flox}$ alleles in ductal cells occurs "catastrophically" while acinar cells utilize a linear progression.

PDAC is commonly and classically hypothesized to go through various stages of mPanIN before developing into PDAC (Hruban et al., 2000). An alternate model termed "catastrophic" progression was proposed in 2003, which suggests that specific stages may be bypassed to rapidly progress into PDAC (Real, 2003). Current findings suggest that acinar cells likely follow the classical model, while the ductal cell model may either undergo a catastrophic progression or classical model of PanIN progression depending on the genetic context.

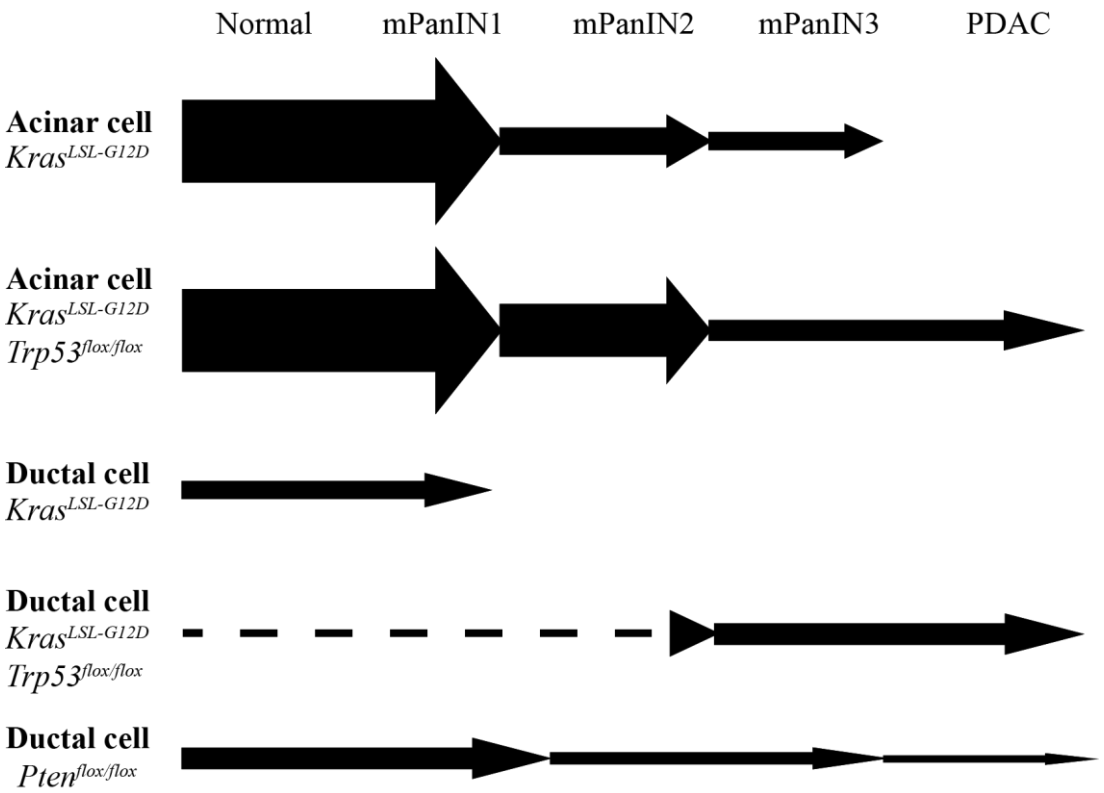

Figure A.1 Summary of PDAC initiation and mPanIN development from ductal and acinar cells.

Acinar cells have been repeatedly shown to follow the classic mPanIN progression scheme. Oncogenic $Kras^{G12D}$ initiates mPanIN formation, and further tumor suppressor loss (eg. *Trp53*) promotes accumulation and progression of mPanIN stages. Kopp et al. (2012) has shown that ductal cells are largely resistant to oncogenic $Kras^{G12D}$. My study has now provided evidence that additional tumor suppressor loss (*Trp53*) initiates high-grade lesions rapidly without going through low-grade lesions (dashed line). Furthermore, unpublished data from our lab shows that ductal cells lacking *Pten* expression can give rise to low-grade mPanIN lesions and initiate PDAC.